Retromer retrieves the Wilson Disease protein, ATP7B from lysosomes in a copper-dependent mode

Santanu Das, Saptarshi Maji*, Ruturaj*, Tanusree Saha*, Indira Bhattacharya, Arnab Gupta[#]

Department of Biological Sciences, Indian Institute of Science Education and Research Kolkata, Mohanpur-741246, India

* Contributed equally

[#] Correspondence to Arnab Gupta: arnab.gupta@iiserkol.ac.in

Abstract: ATP7B utilizes lysosomal exocytosis to export copper from hepatocytes. We investigated the fate of ATP7B, post-copper export. At high copper ATP7B traffics to lysosomes and upon subsequent copper chelation, returns to Trans Golgi Network. At high copper, ATP7B co-localizes with lysosomal marker, Lamp1 and the core member of retromer complex, Vps35. Knocking down VPS35 did not alter copper-responsive vesicularization of ATP7B; rather upon subsequent copper chelation, ATP7B failed to relocalize to TGN that could be rescued by exogenously overexpressing wtVPS35. On testing a series of sorting-motif mutants of ATP7B, we found that deleting the conserved N-terminal motif NXXY, phenocopies trafficking phenotype of ATP7B in VPS35 KD condition and is the possible site of retrograde trafficking regulation. Using super-resolution microscopy we show that VPS35 and ATP7B are juxtaposed on the same lysosomal compartment and their interaction is indirect. We demonstrate that retromer regulates lysosome to TGN trafficking of a non-resident lysosomal cargo, viz., ATP7B and it is dependent upon cellular copper.

Keywords: *ATP7B, retromer, VPS35, copper metabolism, lysosome*

Introduction

Lysosomes have traditionally been believed as a disposal organelle of the cell. A growing body of recent studies have implicated lysosomes as centers of cellular nutrient recycling (Abu-Remaileh et al., 2017; Korolchuk and Rubinsztein, 2011; Rabanal-Ruiz and Korolchuk, 2018). There are growing evidences that lysosomes regulate cellular homeostasis of various metals like, Cu, Zn and Fe. Polishchuk et al. 2014, Blaby-Haas and Merchant 2014, Kurz et al. 2011, Kambe 2011). Copper, a transition metal serves as an essential micronutrient for biological system. It participates in redox reactions in different cellular metabolic pathways shuttling between Cu(II) and Cu(I) states (Uauy et al. 1998), where Cu^{1+} is favored for normal physiological activities (Fahrni 2013). Several proteins tightly regulate copper homeostasis and supplies bioavailable copper to the secretory pathway. Excess copper induces oxidative stress through Fenton reaction and hence is detrimental for living system (Gupta and Lutsenko 2009). Copper homeostasis is primarily maintained by two Trans Golgi Network (TGN) recycling P-type ATPase ATP7A (Menkes Disease Protein) and ATP7B (Wilson Disease Protein). ATP7A is expressed ubiquitously whereas expression of ATP7B is limited to liver, brain and kidney Telianidis et al. (2013) ATP7B solely functions to maintain the copper homeostasis in hepatocytes (Muchenditsi et al. 2017). Defects in ATP7B leads to Wilson Disease (WD), a phenomenon characterized with copper accumulation in liver, brain and other organs manifesting severe hepatic or neurological symptoms (Huster and Lutsenko 2007).

In this study we have attempted to dissect the trafficking itinerary of ATP7B and its mode of regulation in hepatocytes. At physiological/ basal copper level, ATP7B primarily resides on membrane of Trans Golgi Network (TGN) and functions in secretory pathway by delivering copper to Cu dependent ferroxidase enzyme, ceruloplasmin (Lutsenko 2016) within the lumen

of TGN. At higher intracellular copper it vesicularizes (Anterograde trafficking), sequestering copper inside vesicles and exports copper in lysosomes (Polishchuk et al. 2014). What is the fate of copper in the lysosome is still to be determined. It is possible that the entire copper in the lysosome is excreted out of the cell by exocytosis. Alternatively, lysosomes may act as storehouse of bioavailable copper that is tapped as per the requirement of the cell.

Since some recent studies have shown that membrane cargoes recycle back from lysosomes (Seaman 2007; Suzuki and Emr 2018a; Canuel et al. 2008), we examined the fate of ATP7B at the lysosome. We specifically asked (a) Is ATP7B degraded at the lysosome during its copper export activity and (b) If not, what is the mechanism that retrieves ATP7B from lysosomal compartments?

Over 300 mutations in ATP7B are associated with WD and are frequently used to understand regulation and structure-function correlation of ATP7B (Aggarwal et al. 2013); (Gupta et al., 2005), Ala et al. 2015), Ala et al. 2005), Abdelghaffar et al. 2008), Braiterman et al. 2014), Caca et al. 2001). These reported disease mutations affect the functioning of ATP7B either by affecting its copper transporting activity or its trafficking or both (Braiterman et al. 2014, Gupta et al. 2011). Mentionable is the N41S at N-terminus, a naturally occurring WD mutation, which localizes at the TGN and basolateral membrane in all copper conditions (Braiterman et al. 2009). Another disease variant, Arg875 in the A-domain fails to escape ER but can be rescued with copper supplementation (Gupta et al., 2011).

Several proteins govern trafficking and stability of ATP7B (Materia et al., 2012; Jain et al., 2014; Gupta et al., 2018) that interact directly or indirectly with defined and conserved motifs of the protein. These motifs influence the directionality of cargo transport between organelles like Golgi-endosome-plasma membrane. Both ATP7A and ATP7B harbors endocytic di/tri-leucine

68 motif in their C-terminus which facilitates their transport across various compartments (Petris et
69 al., 1998, Braiterman et al., 2011). Francis et al have demonstrated that di-leucine motif
70 ^{1487}LL^{1488} of ATP7A to be important for its retrieval from cell membrane (Francis et al. 1999).
71 Similarly, the ATP7B di-leucine mutant ^{1454}LL>AA^{1455} caused redistribution of ATP7B from TGN
72 to plasma membrane and dendritic vesicles and loss of somatodendritic polarity in rat
73 hippocampal primary neurons (Jain et al. 2014).

74 Although the anterograde pathway of ATP7B has been moderately characterized (Gupta et al.
75 2016, Gupta et al. 2018), the regulation which mediates its retrograde transport from lysosomes
76 has been elusive. Recent studies have shown that retromer regulates retrieval or rescue of
77 cargoes from endosomal and lysosomal compartments (Burd and Cullen, 2014; Gershlick and
78 Lucas, 2017; Lucas and Hierro, 2017; Tammineni et al., 2017). Retromer is a highly conserved
79 endosomal sorting complex, composed of core components, VPS35, 26 and 29 and variable
80 components, Sorting Nexins (SNX) and WASH complex, that are involved in the retrieval and
81 retrograde transport of endocytosed transmembrane proteins (cargoes) to the trans-Golgi
82 network (TGN) or cell surface (Seaman, 2018; Suzuki et al. 2019). The ATP7B homologue,
83 ATP7A, has been shown to be regulated by SNX27 (Cullen and Korswagen, 2012; Steinberg et
84 al., 2013). In rat primary neurons SNX27, a variable member of the retromer complex, rescues
85 neuroligin 2 from lysosomal degradation (Binda et al., 2019). Similarly, SNX17 protects integrin
86 from degradation by sorting between lysosomal and recycling pathways, though retromer is not
87 directly involved. Recycling of CI-M6PR, the protein which delivers acid hydrolases to lysosome,
88 to TGN is dependent on Retromer (Seaman, 2007). Studies from Emr group have shown that in
89 yeast proteins like autophagy protein Atg27 is recycled from vacuole to the endosome via the
90 Snx4 complex and then from the endosome to the Golgi via the retromer complex (Suzuki and

Emr 2018b). Further they have also demonstrated that both VPS26 and VPS35 are critical in cargo retrieval; however VPS26 utilizes different binding sites depending on the cargo, allowing flexibility in its cargo selection (Suzuki et al., 2019) . Besides TGN delivery, retromers also regulate endosome-to-plasma membrane recycling as in Ankyrin-repeat domain 50, ANKRD50 (McGough et al. 2014).

In this study, we have demonstrated that the recycling Cu-P-type ATPase, ATP7B, whose localization in the cell is dictated by intracellular copper levels, recycle from lysosome to TGN upon copper removal and this phenomenon is regulated by the retromer. We have demonstrated that similar to as in case of an endocytic cargo (Mellado et al., 2014, Tabuchi et al., 2009) retromer also sorts a secretory cargo, i.e., ATP7B for its TGN delivery from lysosomes and late endosomes.

Results

ATP7B recycles between Lysosomes and Trans Golgi Network in a copper dependent manner

ATP7B vesicularizes from trans-Golgi network in response to high copper. To determine the optimal time of complete retrieval of ATP7B from vesicles to TGN, HepG2 cells (human hepatocellular carcinoma cell line) were treated with high copper (50µM; 2h) and subsequently treated with 50µM BCS for varying time periods (10min, 30min and 2h). Gradual increase in colocalization between TGN and ATP7B was observed with 10 min, 30 mins and 2h of BCS treatment as evident from Pearson's Colocalization Coefficient (PCC). At 2h, maximum TGN retrieval of ATP7B was observed (Fig. 1, A and B).

Polishchuk et al have demonstrated that ATP7B utilizes lysosomal exocytosis to export copper (Polishchuk et al., 2014). We investigated if ATP7B degrades at the lysosome after it transports copper or it recycles back from lamp1 positive lysosomal compartments for a next round of export cycle. We treated the cells with either BCS (50µM) or increasing amounts of copper (50µM and 250µM). Using immunofluorescence assay we determined that under high copper conditions ATP7B exits TGN and colocalizes with Lamp1 and to a lesser extent with Rab7 positive compartments (Fig. 2, A and B and Fig. S1, A and B). Upon treatment with 250uM copper, a drop of ATP7B protein abundance was observed compared to the two other experimental conditions indicating possible degradation (Fig. 2, C and D). Upon triggering the retrograde pathway with BCS for 30 mins (50µM), for cells that were pre-treated with 50uM copper, we noticed loss of colocalization of lamp1 and ATP7B, indicating lysosomal exit of ATP7B upon copper chelation (Fig. 2A). We did not observe appreciable colocalization of recycling marker, Rab11 and ATP7B (Fig. S1C). Interestingly irrespective of copper treatment we observed a fraction of ATP7B consistently colocalizing with lamp1.

Lamp1 typically marks the terminal end of the endo-lysosomal pathway (Humphries et al., 2011), but frequently, Rab7 and Lamp1 also co-labels the common non-degradative lysosomal compartment (Cheng et al., 2018). To determine the percentage distribution of ATP7B in the milieu of lysosomes-late endosomal compartments (lamp1-Rab7), we utilized Structured Illumination Microscopy (SIM) along with deconvolution confocal microscopy imaging. At elevated copper (50µM) we found a proportionately higher co-distribution of ATP7B with compartments positive for both Rab7 and Lamp1 than compartments positive for individual unique markers. At this condition, 48.5% ± 13.2 of total ATP7B colocalized with either Lamp1 or Rab7 or both. Among them, 44.9% ± 14 of ATP7B localized in vesicles positive for both Lamp1

and Rab7. Hence, it may be inferred that recycling of ATP7B to TGN upon Cu chelation is largely from non-degradative transitory type vesicles which are positive for both the markers than classical lamp1-only lysosomal compartments (Fig. 3, A and B). Together this result suggests that ATP7B localizes at late endo-lysosomal compartments at high copper. However, at this point we could not determine whether the retrograde pathway of ATP7B can also originate exclusively from lysosomal or late endosomal compartments.

It is worth mentioning that the size and shapes of the lysosomal compartments (Lamp1 +) are variable across cells and as well as in a single cell. It varies from 20-200μM in diameter (maximum length across) and shape varies from small puncta to larger patchy clumps. We did not notice any correlationship between size and shape of the compartment with the treated copper concentration or the passage number of the cell.

Retromer regulate retrograde trafficking of ATP7B from lysosome and late endosome

ATP7B exits lysosomes by an unknown regulatory mechanism upon copper chelation. It has been shown that Menkes disease protein, ATP7A, the homologue of ATP7B require SNX27-retromer to prevent lysosomal degradation and maintain surface levels and localization (Steinberg et al., 2013) . Also, CI-M6PR (a constitutive lysosomal recycling cargo) recycles to TGN from lysosomes in a retromer regulated fashion (Arighi et al., 2004; Cui et al., 2019). This prompted us to investigate if the retromer complex plays a role in retrieval of ATP7B (a non *bona fide* lysosomal cargo) from lysosome and late endosomal compartments. VPS35 is the largest core component of the retromer complex. It functions as the scaffold for the assembly of other core components, VPS29 and VPS26 and also cargo binding (Hierro et al., 2007). Hence, we selected hVPS35 as the target component to determine the role of retromer complex, if any in copper mediated trafficking of ATP7B.

158 Broadly, localization and trafficking of ATP7B in HepG2 can be divided in 4 *phases* (a) at the
159 TGN in Basal Cu (or –Cu), (b) on the anterograde vesicles in high Cu and (c) on the retrograde
160 vesicles in high Cu > Cu chelated conditions (10 mins BCS treatment) and (d) majority of ATP7B
161 back to the TGN in high Cu > Cu chelated conditions (30 mins/2h BCS). Immunoblot analysis of
162 VPS26 and VPS35 revealed that HepG2 cells expresses the retromer complex proteins (Fig.
163 4A) and copper does not alter abundance of VPS35 in HepG2 cells (Fig. S2A)

164 To study if ATP7B co-localizes with retromer core components, cells were treated with either of
165 the 4 conditions described above. Cells were fixed, blocked and co-stained with anti-ATP7B and
166 anti-VPS35 or anti-VPS26 antibody. Maximum colocalization as quantified by Pearson's
167 Colocalization Coefficient between VPS35 and ATP7B was observed in Cu (2h)>BCS (10min)
168 (*phase c*) followed by high copper condition (*phase b*) condition. Further with 30 min BCS
169 treatment post high copper (*phase d*), ATP7B and VPS35 shows loss of colocalization (Fig. 4,
170 B and C). Similar observations were made with VPS26 (data not shown).

171 To further understand if retromer regulates any of these phases of ATP7B trafficking, we
172 knocked down VPS35 and studied the phenotype of copper induced localization of ATP7B with
173 respect to TGN. Appreciable knockdown was attained (>70-80%) for the targeted siRNAs as
174 compared to scrambled for VPS35 as ascertained by immunoblotting (Fig. 5A). Furthermore, as
175 reported by (Fuse et al.,2015) decrease in expression of VPS26 was also observed in VPS35
176 KD cell which eventually tells us expression as well as functionality of VPS subunits are
177 interdependent (Fig. S2B).

178 VPS35 siRNA treated cells were incubated with (a) BCS or (b) Copper or (c) Copper > BCS (30
179 min), fixed, blocked and stained with the anti-ATP7B and anti-Golgin97 antibodies. We observed
180 that trafficking of ATP7B from the vesicles back to the TGN (*condition c*) was significantly

abrogated (Fig. 5, B and C and Fig. S2C). ATP7B remained in vesicles and failed to recycle back to TGN even after the cells were incubated in BCS for a prolonged time of 2h subsequent to copper treatment (not shown).

To corroborate our finding that VPS35 regulates ATP7B trafficking, we utilized the wild type and the inactive dominant negative mutant mCherry-VPS35 (R107A) (gift from Dr, Sunando Datta, IISER Bhopal). The R107A mutation abolishes the interaction of VPS35 with VPS26 and affects cargo sorting. (Gokool et al., 2007; Zhao et al., 2007) . Cells were co-transfected with GFP-ATP7B and mCherry-wt-VPS35 and GFP-ATP7B was concentrated at TGN (perinuclear region) with copper chelator. Vesicularization and recycling of ATP7B was triggered with treatment with copper. Image capture was initiated at the point of copper treatment and data was collected at an interval of 1.93 second for a total period of 30 mins. We noticed that within 1 min of Cu treatment, GPF and m-Cherry signals colocalized at the same endosomal vesicle. The dwell time of wt-VPS35 and GFP-ATP7B on the vesicle was significantly higher for wt-VPS35 compared to the mutant. For VPS35-R107A, the colocalization lasted for few seconds (4-11 seconds) but for wt-VPS35, the colocalization lasted for an average of 7 mins. (Video 1, A and B) and (Fig. S3, A and B).

Since we determined that ATP7B colocalizes at the lysosomes at high copper, we investigated if VPS35 regulates lysosomal exit of ATP7B on triggering its retrograde pathway. Using identical experimental conditions of knocking down VPS35, we found that ATP7B is arrested at lysosome upon triggering the retrograde pathway (i.e., high copper > BCS) (Fig. 5D). Interestingly, boosting the retrograde pathway by lengthening BCS treatment time to 2h did not facilitate retrieval of ATP7B from the lysosomes (Fig. 5D). Also, in VPS35 kd cells, a population of ATP7B

was arrested in late endosome (Rab7 positive) upon activating the retrograde pathway (Fig. S2C).

We confirmed the role of retromer by rescuing the non-recycling phenotype of ATP7B in VPS35 kd cells by overexpressing mcherry-wt-VPS35. We found that ATP7B recycled back from vesicular to its tight perinuclear TGN localization upon copper chelation in VPS35 kd cells that overexpressed the wt-VPS35 construct (Fig. 5E). These experiments confirm that VPS35 regulates retrieval of ATP7B from lysosomes (and also possibly from late endosomes) to TGN upon copper depletion.

Lysosomal luminal pH does not influence localization of ATP7B and recruitment of VPS35

It emerges that copper induced localization of ATP7B involves a tripartite participation, i.e., ATP7B, lysosome and retromer. After confirming the role of VPS35 in this process, we asked if luminal lysosomal environment affect retromer recruitment and hence ATP7B retrieval from lysosome. Retromers have been previously implicated in lysosomal activity e.g., autophagy (Cui et al., 2019) . We investigated if the targeting of ATP7B to lysosomes in high copper or its retrieval initiation by VPS35 recruitment is affected by inactivation of the V-ATPase that is crucial for lysosomal functioning. Cells were treated with the V-ATPase inhibitor, BafA1, in 50μM copper (to trigger lysosomal targeting of ATP7B) and Cu>BCS (20 mins) conditions (to trigger its lysosomal exit). No observable and significant difference in colocalization of Lamp1, ATP7B and VPS35 was obtained between BafA1 treated vs the control in either condition. It can be inferred that retromer being situated on the outer membrane of the Lamp1 positive compartments is unaffected by the change in luminal pH of the lysosome brought on by BafA1 treatment. Localization of ATP7B also stays unaltered as also demonstrated by Polishchuk et al. (Fig. 6)

ATP7B N-terminal ^{41}NVGY^{44} (NXXY motif) mutant phenocopies VPS35 knockdown

We wanted to identify the ATP7B motif(s) that regulates its retrograde trafficking. Since, there are no signature retromer regulatory motifs on cargoes yet reported, at the outset, we did an unbiased search using published literatures of sorting signals. We found 3 strong sorting motifs, one on N-terminal (^{41}NXXY^{44}) and two on the C-terminal (^{1376}YXXϕ^{1384} and ^{1454}LLL^{1456}) that are conserved across species (Fig. S4A). The YXXϕ is repeated thrice in tandem (1373-1384 residue). We mutated the three N and C terminal motifs (Table S4B) and observed if any of these mutants phenocopy trafficking behavior of ATP7B in VPS35 knocked down cells. The ΔNVGY-ATP7B localizes at the TGN in BCS and traffics to lysosomes (Lamp1+ and VPS35+) at high copper. Interestingly, it fails to recycle back to the TGN when copper is chelated by BCS, a phenotype identical to VPS35 KD condition (Fig. 7). The C-terminus ^{1454}LLL^{1456}>AAA mutant as previously reported constitutively vesicularizes in all the three condition (Braiterman et al., 2011). The second C-terminus mutant ΔYXXϕ shows primarily ER like staining with some vesicles in all the three conditions. Hence we did not proceed further with C-terminal mutants (Fig. S4C). From the phenocopy experiment we can infer that retrograde trafficking of ATP7B is most likely regulated via the NXXY (NVGY in ATP7B) motif of N-terminus. The NVGY motif harbors a Wilson Disease mutation (N41S) that has been shown to be missorted in high copper conditions (Braiterman et al., 2009) . We also found that though the level of expression was lower than the wt-ATP7B, ATP7B-N41S faithfully replicates the non-returning phenotype as observed in VPS35 knockdown condition (Fig. S4C). In copper limiting condition it primarily localized to TGN and a few vesicles. In addition, on mutating the other invariant residue Tyr^{44}, i.e., Y44V and the putative phosphomimetic Y44D, ATP7B exhibited ER localization (Table. S4B).

VPS35 acts on ATP7B in a micro-distant *modus operandi*

Next, using biochemical assays we investigated if VPS35 directly interacts with N terminus of ATP7B (harboring NXXY motif). The GST-tagged 1-650 amino acid (with all 6 MBRs) N-terminus ATP7B construct (+Cu and –Cu) that was used as bait was immobilized on GSH beads to fish out VPS35 from HepG2 lysate. On probing with anti-VPS35 antibody, we failed to detect any interaction. The C-terminus ATP7B was used as a negative control (Fig. S5A, i-vi). Further we utilized co-immunoprecipitation where GFP-ATP7B was expressed in cells, pulled down with anti-GFP beads and probed for endogeneous VPS35. We did not observe any interaction (Fig. S5B, vii-viii).

To understand the underlying reason of why we could not detect interaction between ATP7B and VPS35 using biochemical methods, we resorted to Super resolution microscopy to determine the exact positioning of ATP7B w.r.t VPS35 at the lysosomal compartment. Using Structured Illumination Microscopy and High resolution deconvolution confocal microscopy we observed that ATP7B and VPS35 lies in juxtaposition on the lysosomal compartment (stained with Lamp1 antibody) at high copper conditions (Fig. 8, A-D). The average distance between these two proteins varies from 25nm~200nm. It can be inferred that although ATP7B lies in close proximity to VPS35 and is regulated in its retrograde pathway by retromer, the physical interaction between these two proteins are indirect. We utilized Stimulated Emission Depletion (STED) microscopy to look further closely on the disposition of ATP7B and Vps35 on a vesicular membrane. Using Z-stacking we determined the shape of a vesicle (dotted circle in Fig. 8E) and observed that ATP7B (green) and Vps35 (red) decorated the vesicular membrane with minimal signal overlap (yellow) at a maximum resolution of 25nm further substantiating our biochemical findings.

In summary we establish that, ATP7B traffics to lysosomes at high copper where it juxtaposes with VPS35, the core member of the retromer complex. Upon triggering the retrograde pathway by subsequent copper chelation, retromer regulates the recycling of ATP7B from the lysosome to the TGN (Fig. 9).

Discussion:

The copper transporting ATPase, ATP7B exports copper through lysosomes. ATP7B (160kDa) is a large 8 membrane spanning protein with a total of 1465 residues. ATP7B resides on the TGN membrane at basal copper levels and traffics to lysosomes and Rab7 compartments at high copper. We argue that it would be highly wasteful for the cell to degrade ATP7B after each cycle of copper export from the TGN to the lysosomes. We wondered whether ATP7B recycles back from the lysosome after it pumps copper in the lysosomal lumen for either export out of the cell or for reutilization as a nutrient that requires to be investigated. Interestingly, the protein does not get degraded unlike most other cargoes that are destined for degradation at the lysosomes. The luminal loops of ATP7B between the 8 TM domains are small and probably escapes lysosomal hydrolases. Also, low pH in lysosomal lumen might help the release of copper from the His residues that are located between TM1-TM2 loop as shown in its homologue ATP7A (Barry et al., 2011; LeShane et al., 2010; Otoikhian et al., 2012) and binds copper.

Further we asked what might be the regulator(s) that affects ATP7B's recycling back from the lysosome. In a preliminary proteome analysis on GFP-ATP7B vesicles isolated from HepG2 cells (data not shown), we have identified members of the retromer complex. Previously (Harada et al., 2000) had shown that ATP7B resides in late endosome (Rab7 positive) in high copper. Retromer on the other hand is recruited on endosomal membrane by sequential action of Rab5 and Rab7 (Rojas et al.. 2008). Further, Priya et al., 2015 dissected the interaction of Rab7 and

retromer complex and demonstrated that Rab7 recruits retromer to late endosomes via direct interactions with N-terminal conserved regions in VPS35.

Before investigating the role of retromer in retrieval of ATP7B from lysosomes, we first determined if ATP7B is stable in lysosomal and Rab7 compartments. Interestingly it was reported by Polishchuk et al, that even up to 200uM copper treatment in HepG2 cells, ATP7B shows no significant degradation. However, we noticed a drop in ATP7B abundance indicating degradation at 250uM copper at 2 hrs though the cellular architecture apparently looks normal under phase contrast microscope. At 50µM copper, ATP7B did not exhibit any degradation.

Upon examining triple-colocalization of ATP7B, VPS35 and Lamp1 in fixed cells, we notice that the level of overlap is moderate at high copper. This might be attributed to the fact that at a given point in copper treated cells, the nature of vesicles are highly heterogeneous comprising of retrograde and anterograde vesicles and that too at various stages of trafficking. We hypothesize that the lysosomes would exhibit a higher co-residence of VPS35 and ATP7B if we are able to synchronize the TGN exit (upon copper treatment) and lysosomal exit (upon subsequent copper removal) of ATP7B. However, time lapse imaging showed that GFP-ATP7B and mCherry-Vps35 colocalizes in the compartment for a few minutes. In VPS35 kd cells, ATP7B is trapped in the lysosomes even upon activating the retrograde pathway (Copper>BCS). We reason that ATP7B recycles back to TGN from the lysosomes directly and not via plasma membrane as we did not observe ATP7B staining at the plasma membrane or even at the cortical actin (data not shown).

Interestingly, we did not detect any direct interaction of ATP7B and VPS35 (or VPS26). This is possibly due to the fact that though retromer complex regulates lysosomal exit of ATP7B, the interaction is mediated via a different member of the complex. Retromer complex shows heterogeneity in its subunits that are responsible for binding to the cargo (Follett et al., 2016;

Zhang et al.,2012; Suzuki et al., 2019; Belenkaya et al., 2008; Feinstein et al., 2011). It has been shown that the canonical recycling signal for the Divalent Cation Transporter (DMT1-II) binding of retromer is mediated via the interface of VPS26 and SNX3 in a hybrid structural model shows that the α-solenoid fold extends the full length of Vps35, and that Vps26 and Vps29 are bound to its two opposite ends (Lucas et al., 2016; Hierro et al., 2007). This extended structure suggests that multiple binding sites for the SNX complex and receptor cargo are present. It has been shown show that membrane recruitment of retromer is mediated by recognition of SNX3 and RAB7A, by the VPS35 subunit. These bivalent interactions prime retromer to capture integral membrane cargo, which enhances membrane association of retromer and initiates cargo sorting (Zhao et al., 2007). Further studies are needed to be carried out to identify the exact interface of ATP7B-retromer interaction.

How copper (or copper removal) mediates triggering of ATP7B's retrograde pathway is not understood. It is likely that copper binding to the 6 MBD on ATP7B N-terminus, exposes the upstream 1-63 N-terminal domain containing the ^{41}NXXY^{44} domain. This relaxed N-terminus 1-63 conformation might be favorable for it to interact with the retromer complex. We demonstrate in our phenocopy experiments that mutations on this domain traps the protein in lysosomes. As also determined in our experiments, it is unlikely that motifs on the C-terminal (tandem ^{1373}YXXϕ^{1384} and ^{1454}LLL^{1456}) or other cytoplasmic domains would be serve as copper dependent retromer regulatory motifs of ATP7B due to lack of any copper binding sites in its proximity. However, role of C-terminus cannot be completely discounted as Braiterman et al has shown that multiple regulatory phosphorylation sites lie on the C-terminus that might play an indirect role in regulation of ATP7B by retromer complex (Braiterman et al., 2015).

Wilson disease, though a Mendelian disorder caused by mutations only in *ATP7B* gene, shows a large spectrum of symptoms and age of onset. We hypothesize that polymorphisms and mutations in trafficking regulatory proteins might be responsible for imparting such high phenotypic heterogeneity. Mutations and SNPs in the retromer subunit genes are associated with many hereditary conditions (Reitz 2018; Small 2008; Chen et al., 2017; Rahman and Morrison 2019; Shannon et al., 2014). Varadarajan et al, reported significant association of SNPs of retromer complex genes (SNX1, SNX3 and Rab7A) with Alzheimer's disease Vardarajan et al., 2012) Similarly, VPS35 hemizygous condition accentuates Alzheimer's disease neuropathology (Wen et al., 2011). Additionally, Parkinson's disease-linked *D620N VPS35* knockin mice manifest tau neuropathology and dopaminergic neurodegeneration (Chen et al., 2019). It would be important to extend the knowledge of role of retromers in ATP7B trafficking to delineate genotype-phenotype correlationship in Wilson disease patients.

Acknowledgments

This work was supported by Wellcome Trust India Alliance Fellowship (IA/I/16/1/502369) and Early Career Research Award (ECR/2015/000220) from SERB, Department of Science and Technology (DST), Government of India and IISER K intramural funding to AG. SM and IB was supported by Pre-doctoral fellowship from Council of Scientific and Industrial Research, India. TS was supported by National Postdoctoral Fellowship, SERB, India. We thank Dr. Ashima Bhattacharjee for critical review of the manuscript.

Author contributions: AG and SD designed the experiments and wrote the manuscript. SD, Ruturaj and TS did the experiments and analyzed the data. SM wrote the codes and analyzed the data. Ruturaj helped with time-lapse imaging. IB conducted the experiments with the ATP7B

mutants. Dr. Anupam Banerjee (Zeiss) helped us with SIM imaging at JNCASR. STED microscopy was carried out at the Leica microscopy facility at IISER Pune. All authors reviewed the results and approved the final version of the manuscript.

We thank Rahul Das (IISERK), Arindam Mukherjee (IISERK), Oishee Chakrabarti (Saha Inst of Nuclear Physics), Ashima Bhattacharjee (Amity Univ. Kolkata) for sharing their reagents and instruments with us.

The authors declare no competing financial interests.

370 # Materials and methods

371 ## Plasmids and reagents

372 GFP-ATP7B construct was available in lab. The mCherry WT-VPS35 and mCherry VPS35
373 (*R107A*) construct was kindly gifted by Dr. Sunando Datta, IISER Bhopal, India. pET28aSUMO
374 and pGEX vectors was kindly gifted by Dr. Rahul Das, IISER-Kolkata, India.Following are the
375 antibodies that has been used for experiments: rabbit anti-ATP7B (# ab124973), mouse anti-
376 golgin97 (# A21270), goat anti-VPS35 (# NB 100-1397), mouse anti-VPS26 (# NBP 236754),
377 mouse anti-VPS35 (# sc-374372); for western blot, mouse anti-Lamp1 (DSHB: # H4A3), mouse
378 anti-Rab7 (# sc-376362), Donkey anti-Rabbit IgG (H+L) Alexa Fluor 488 (# A-21206), Goat anti-
379 Rabbit IgG (H+L) Alexa Fluor Plus 647 (# A32733), Donkey anti-Mouse IgG (H+L) Alexa Fluor
380 Plus 647 (# A32787), Donkey anti-Goat IgG (H+L) Alexa Fluor 568 (# A-11057), Donkey anti-
381 Mouse IgG (H+L) Alexa Fluor 568 (# A10037). Endo toxin free plasmid isolation was done using
382 EndoFree Plasmid Maxi Kit (# 12362).

383 ## Cell lines and cell culture

384 HepG2 cells were grown and maintained in complete medium containing low glucose Minimum
385 Essential Medium (MEM) (# 41500-034) supplemented with 10% Fetal Bovine Serum (# 10270-
386 106), 1X Penicillin-Streptomycin (# A001), 1X Amphotericin B (# 15290026). Similarly HEK293T
387 cells were grown and maintained in Dulbecco's modified Eagle's medium (DMEM) (#
388 CC3004.05L) supplemented with 10% Fetal Bovine Serum,1X Penicillin-Streptomycin, 1X
389 Amphotericin B. For transfection of plasmids in HepG2 cell, Lipofectamine 3000 reagent (#
390 L3000-001) was used according to manufacturer's protocol. For transfection in HEK293T, for
391 live cell imaging, JetPrime (# 114-07) transfection reagent was used.

392 **Knockdown assays**

393 Accell Human VPS35 (55737) siRNA-SMARTpool (#E-010894-00-0010), Accell Non-targeting
394 siRNA (#D-001910-01-05), Accell siRNA Delivery Media (#B-005000-100), 5X siRNA Buffer (#B-
395 002000-UB-100) and Molecular Grade RNase-free water (#B-003000-WB-100) were purchased
396 from Dharmacon. HepG2 cells were seeded in complete medium at a density of 1.5×10^5 cells/ml
397 in coverslips heat fixed on 24-well plate. Cells were allowed to double for approx. 48hrs (doubling
398 time of HepG2). After 48 hours, media was discarded, rinsed with 1X PBS pH 7.4 and si RNAs
399 were added at a final concentration of 1µM resuspended in Accell siRNA Delivery Media (# B-
400 00-5000-100). This condition was maintained for 72 hours after which the si-RNA containing
401 media was replaced with complete media and again maintained for another 24 hours. This
402 ensures better knock down at protein level. To validate knock down of VPS35, western blot was
403 performed following same protocol from one well of 24 well plate.

404 **Immunofluorescence**

405 HepG2 cells were seeded at a density of (0.8-1.6×10^5 cells/ml) on coverslips heat fixed on wells
406 of 24 well plate each time while conducting immunofluorescence. Any treatment was performed
407 at a confluency of (60-70) %, including transfection. 4% Para-formaldehyde (PFA) fixation was
408 done following treatment. After fixation cells were permeablized with chilled methanol and finally
409 washed with 1X PBS. Fixation and permeablisation was carried out in cold condition. Cells were
410 blocked in 3% BSA suspended in 1X PBS for either 2hours at room temperature (RT) or O/N at
411 4^{o}C. Following this, primary antibody (1^0) incubation was done at RT in moist chamber for
412 2hours. After 1^0 incubation, cells were washed with 1X PBST for 3 times and again re-incubated
413 with corresponding secondary antibodies (2^0) for 1.3 hours at RT. This was followed by further
414 washing with 1X PBST for 3 times and finally with 1X PBS for two times. Coverslips were fixed

on glass slides using SIGMA Fluoroshield™ with DAPI mountant. (#F6057). The solvent for antibody suspension was 1% BSA in 1X PBST.

For STED sample preparation, HepG2 cells were seeded on glass coverslips, treated with BCS and copper (as mentioned in Fig. 8E). Treatment was done at 70% confluency. Cell were fixed with 2% PFA for 20mins followed by washing with 1X PBS, pH 7.2 for 15mins (× 2) and then quenched with 50mM NaCl. Blocking and permeation was done for 30mins with 1% BSA along with 0.075% saponin. Cell were co-incubated with primary rabbit anti-ATP7B and goat anti-VPS35 for 2hrs at room temp. Followed by 1X PBS washing and incubation with secondary anti-rabbit Alexa 488 and anti-goat Alexa 647. Coverslips was mounted with ProLong™ Diamond Antifade Mountant with DAPI (# P36962).

Time-lapse fluorescence microscopy

HEK293T cells were seeded on confocal dishes (SPL) and were co-transfected separately with GFP-ATP7B and mCherry-VPS35-WT, mCherry-VPS35-MT(R107A) (gift by Sunando Datta, IISER Bhopal), using jetPRIME (Polyplus) transfecting regent as per manufacturer protocol. Images were acquired using Leica SP8 confocal setup with 63x oil objective. For ATP7B & VPS35-WT/MT, images were taken at every 1.964 s interval using Lightning by Leica .All the images were processed using Fiji and LASX software provided by Leica and videos were processed using Cyberlink Powerdirector.

Co-purification assays and co-immunoprecipitation:

Copurification: Composition of bacterial lysis buffer for N-term and C-term ATP7B: 50mM Tris-Cl, 50mM NaCl, 5mM EDTA, 10% glycerol (5% for C-term), ~1mM beta-marcaptoethanol, pH-

8.0. Same buffer was used for the washing after incubation of lysates with beads. Composition of HepG2 cell lysis buffer:1X PBS buffer with 250mM sucrose, 1mM EDTA, 1mM EGTA, 1mM PMSF and 1X protease inhibitor cocktail. Same buffer was used for the washing after incubation of lysates with beads. Wt-C-term and Wt-N-term ATP7B were cloned into the pET28aSUMO and pGEX vectors respectively followed by transformation into competent BL21 E.coli for the bacterial expression of the proteins. BL21 containing Wt-N-term ATP7B was grown in Luria broth in presence of 100µg/ml ampicillin whereas BL21 containing Wt-C-term ATP7B was grown in nutrient broth in presence of 50µg/ml kanamycin followed by induction with 1mM isopropyl β-D-thiogalactopyranoside (IPTG) at 18ºC and 37ºC respectively for 16hr. BL21 and empty pGEX were used as negative control for C-term and N-term ATP7B co-purification respectively. Cells were resuspended in lysis buffer and lysed by sonication (100 amplitude/10 sec on/30 sec off) x 7 to 8 cycles. Bacterial lysates (collected from 100ml culture) were incubated with the Ni-sepharose (for C-term) and GSH Beads (for N-term) for 3hr at 4ºC followed by washing using respective buffers. HepG2 pellet (collected from 10mm dish) was lysed by sonication (100 amplitude/10 sec on/30 sec off) x 5 cycles using respective lysis buffer for C-term and N-term co-purification. Insoluble materials were sedimented at 13,200rpm for 20mins at 4ºC and supernatant was incubated with beads for 3hr at 4ºC followed by elution with 3XSDS-PAGE loading buffer. Eluted products were used for western blotting using anti-VPS35 and anti-VPS26 antibodies.

Co-immunopreciptation: All solutions were pre-chilled to 4°C and all steps were carried out on ice. HEK293T cells were transfected with GFP-ATP7B and treated with different Cu conditions followed by washing with 1x PBS and lysis using lysis buffer (10mM Tris-Cl pH 7.5, 150mM NaCl, 0.5mM EDTA, 0.5 % NP40, PMSF and protease inhibitor cocktail in ddH_2O). Cell extracts

were triturated with 2ml syringe and incubated for total 45minutes and the insoluble materials were sedimented at 16,000*g* for 10 min at 4°C. Co-IP experiment was performed using GFP-trap beads (ChromoTek, # gta-20) following the manufacturer protocol. The supernatants were diluted using diluted buffer (10mM Tris-Cl pH 7.5, 150mM NaCl, 0.5mM EDTA, PMSF and protease inhibitor cocktail in ddH_2O to yield 0.25 % NP40) and incubated with GFP-trap beads for 2hr at 4°C on a rotating wheel. Finally the interacting proteins were eluted using 0.2M glycine and used for western blotting. Western blotting of VPS35, VPS26 and GFP: Samples for Western blotting were resolved by sodium dodecyl sulphate-polyacrylamide gel electrophoresis (SDS-PAGE) and separated proteins were transferred to nirocellulose membrane. After protein transfer, the membrane was blocked in 5% non-fat milk powder (for VPS35&VPS26) and 3% BSA (for GFP) and incubated with primary antibody diluted in 5% non-fat milk powder (for mouse anti-VPS35 & mouse anti-VPS26 1:1500 dilution) or 1%BSA (for rabbit anti-GFP 1:10000 dilution) overnight at 4°C. Following incubation, the membrane was briefly washed three times with TBS-T and incubated with HRP-conjugated secondary antibodies (anti-mouse HRP 1:5000 dilution and anti-rabbit HRP 1:15000 dilution) diluted in 5% non-fat milk powder or 1%BSA for 1.5hr at RT. The membrane was washed three times for 5 min in TBS-T flowed by two times washing with TBS at RT and incubated for 5min at RT with Enhanced Chemiluminescence (ECL) substrate and ECL plus (1:1).

Immunoblotting

HepG2 cells were grown on 60mm dish and cell pellet was collected at 70% confluency. For lysate preparation of membrane protein dry pellet was dissolved in 200µL of lysis buffer (composition: sucrose 250mM, EDTA 1mM, EGTA 1mM, 1X PBS as solvent, 1X protease cocktail inhibitor) and incubated on ice for 1hour with intermittent tapping. Dounce

homogenization of dissolved pellet was done for approx. 400 times followed by syringe up down with 22-24 gauge needle for 20-25 times on ice. This enables the cell to rupture completely. The soup was centrifuged at 600 R.C.F at 4^0C for 10mins to discard debris and nucleus. Further mitochondrial fraction was discarded by centrifugation at 3000 R.C.F for 10mins at 4^0C. The resultant soup was subjected for ultra-centrifugation at 1,00,000 R.C.F for 1hour at 4^0C to collect membrane fraction. Pellet was dissolved in membrane solubilizing buffer (composition: sucrose 250mM, EDTA 1mM, EGTA 1mM, NP-40 1.0%, Triton X-100 1.0%, 1X PBS as solvent, 1X protease cocktail inhibitor). For, soluble protein, whole cell lysate was prepared with RIPA lysis buffer (composition: 10mM Tris-Cl pH 8.0, 1mM EDTA, 0.5mM EGTA, 1.0% Triton X-100, 0.1% sodium deoxycholate, 0.1% sodium dodecyl sulphate, 140mM NaCl, 1X protease cocktail inhibitor). Dry pellet was dissolved in RIPA lysis buffer and incubated on ice for 30mins with intermittent tapping. The solution is then sonicated with a probe sonicator (3-4 pulses, 5sec, 100mA). Followed by this, centrifugation at 20,000 R.P.M for 20mins at 40C was done to pellet down cellular insoluble debris and soup was collected. Protein estimation was carried out with Bradford reagent (B6916-500ML) following manufacturer's protocol. Protein sample preparation was done by adding 4X loading buffer (composition: Tris-Cl pH 6.81, 4% SDS, 10% β-ME, 20% glycerol, 0.02% bromophenol blue, urea 8M) to a final concentration of 1X and ran on SDS PAGE (6% for membrane fraction and 10-12% for soluble fraction) to separate proteins according to molecular mass. This was further followed by wet transfer of proteins onto nitrocellulose membrane (1620112, BioRad). After transfer, the membrane was blocked with 3% BSA in 1X Tris-buffered saline (TBS) buffer pH7.5 for 2hrs at RT with mild shaking. Primary antibody incubation was done overnight at 4^0 C following blocking and then washed with 1X TBST (0.01% Tween-20) for 10mins (× 3 times). HRP conjugated respective secondary

505 incubation was done for 1.3 hrs at RT, further washed and signal was developed by ECL
506 developer (170-5060, BioRad/ 1705062, BioRad) in chemiluminescence by Chemi Doc (BioRad)

507 **Microscopy**

508 All images were acquired with Leica SP8 confocal platform using oil immersion 63X objective
509 and deconvoluted using Leica Lightning software. For Structured Illumination Microscopy,
510 images acquisition was taken at 100X magnification in Zeiss Elyra PSI. For Stimulated emission
511 depletion (STED) microscopy, imaging was done in Leica STED 3X. For Alexa 647, 775 STED
512 laser line was used and for Alexa 488, 592 laser line was used for depletion. Line average was
513 set at 4 and pixel size was kept as 25nm to achieve maximum resolution. STED corrected
514 images were deconvoluted and processed by Scientific Volume Imaging of Huygens
515 Professional Software with default settings.

516 **Image analysis and statistics**

517 Images were analyzed in batches using ImageJ (Schneider et al., 2012), image analysis
518 software. For colocalization study, Colocalization_Finder plugin was used. RO Is were drawn
519 manually on best z-stack for each cell. For three protein colocalization study, the other two
520 protein co-residing vesicles were isolated using Analyze Particle tool, and colocalization study
521 were carried on with the reference protein, ATP7B in our case. RGB_Profiler plugin was used to
522 obtain the line profile graph. For statistical analysis and plotting, ggplot2 (Wickham 2009)
523 package was used in R v-3.4.0 (Team 2015). Non-parametric tests for unpaired datasets
524 (Kruskal Wallis test and Mann-Whitney U test**)** were performed for all the samples.

525

Fig 1: ATP7B & Golgin97 spatiotemporal

	BCS 2hrs	Cu 2hrs	Cu>BCS 10’	Cu>BCS 30’
Cu>BCS 2hrs	**	****	****	****
Cu>BCS 30’	****	****	****	
Cu>BCS 10’	****	ns		
Cu 2hrs	****			

Data set was collected from BCS 2hrs (32 cells), Cu 2hrs (89 cells), Cu>BCS 10’ (46 cells), Cu>BCS 30’ (82cells), Cu>BCS 2hrs (195)

Fig 2: ATP7B & Lamp1 spatiotemporal

	BCS	Cu
Cu>BCS30	****	****
Cu	****	

The dataset was collected from 215 cells for BCS treatment, 150 cells for Copper treatment, 196 cells for Cu>BCS 30’

Fig3: ATP7B & VPS35 spatiotemporal

	BCS	Cu	BCS10
Cu>BCS30	*	**ns**	**ns**
Cu>BCS10	**	**ns**	
Cu	**		

The dataset was collected from 66 cells for BCS treatment, 69 cells for Copper treatment, 54 cells for Cu>BCS10’ and 80 cells for Cu>BCS 30’

Fig4: ATP7B & Golgin97 (siVPS35)

	BCS ctrl	Cu ctrl	Cu>BCS ctrl	BCS si	Cu si
Cu>BCS si	****	ns	****	****	ns
Cu si	****	ns	****	****	
BCS si	ns	****	ns		
Cu>BCS ctrl	****	****			
Cu ctrl	****				

Data set was collected from BCS ctrl (22 cells), Cu ctrl (21 cells), Cu>BCS ctrl (19 cells), si BCS (15 cells), si Cu (15 cells), si Cu>BCS (20 cells)

* P<0.05, ** p<0.01, *** p<0.001, **** p<0.0001, ns- non significant

Online Supplementary materials

Video: Time lapse imaging to record colocalization of ATP7B (green) and VPS35 (red) in high copper. 1A: ATP7B and wt-VPS35; 1B: ATP7B and R107A-VPS35

Bibliography

Abdelghaffar, T.Y., S.M. Elsayed, E. Elsobky, B. Bochow, J. Buttner, and H. Schmidt. 2008. Mutational analysis of ATP7B gene in Egyptian children with Wilson disease: 12 novel mutations. *J Hum Genet*. 53:681-687.

Abu-Remaileh, M., G.A. Wyant, C. Kim, N.N. Laqtom, M. Abbasi, S.H. Chan, E. Freinkman, and D.M. Sabatini. 2017. Lysosomal metabolomics reveals V-ATPase- and mTOR-dependent regulation of amino acid efflux from lysosomes. *Science*. 358:807-813.

Aggarwal, A., G. Chandhok, T. Todorov, S. Parekh, S. Tilve, A. Zibert, M. Bhatt, and H.H. Schmidt. 2013. Wilson disease mutation pattern with genotype-phenotype correlations from Western India: confirmation of p.C271* as a common Indian mutation and identification of 14 novel mutations. *Ann Hum Genet*. 77:299-307.

Ala, A., E. Aliu, and M.L. Schilsky. 2015. Prospective pilot study of a single daily dosage of trientine for the treatment of Wilson disease. *Dig Dis Sci*. 60:1433-1439.

Ala, A., J. Borjigin, A. Rochwarger, and M. Schilsky. 2005. Wilson disease in septuagenarian siblings: Raising the bar for diagnosis. *Hepatology*. 41:668-670.

Arighi, C.N., L.M. Hartnell, R.C. Aguilar, C.R. Haft, and J.S. Bonifacino. 2004. Role of the mammalian retromer in sorting of the cation-independent mannose 6-phosphate receptor. *J Cell Biol*. 165:123-133.

Barry, A.N., A. Otoikhian, S. Bhatt, U. Shinde, R. Tsivkovskii, N.J. Blackburn, and S. Lutsenko. 2011. The lumenal loop Met672-Pro707 of copper-transporting ATPase ATP7A binds metals and facilitates copper release from the intramembrane sites. *The Journal of biological chemistry*. 286:26585-26594.

Belenkaya, T., Y. Wu, X. Tang, B. Zhou, L. Cheng, Y. Sharma, D. Yan, E. Selva, and X. Lin. 2008. The Retromer Complex Influences Wnt Secretionby Recycling Wntless from Endosomesto the Trans-Golgi Network. *Dev Cell.* . 14:120-131.

Binda, C.S., Y. Nakamura, J.M. Henley, and K.A. Wilkinson. 2019. Sorting nexin 27 rescues neuroligin 2 from lysosomal degradation to control inhibitory synapse number. *Biochem J*. 476:293-306.

Blaby-Haas, C.E., and S.S. Merchant. 2014. Lysosome-related Organelles as Mediators of Metal Homeostasis. *J. Biol. Chem.* 289:28129 –28136.

Braiterman, L., L. Nyasae, Y. Guo, R. Bustos, S. Lutsenko, and A. Hubbard. 2009. Apical targeting and Golgi retention signals reside within a 9-amino acid sequence in the copper-ATPase, ATP7B. *Am J Physiol Gastrointest Liver Physiol*. 296:G433-444.

Braiterman, L., L. Nyasae, F. Leves, and A.L. Hubbard. 2011. Critical roles for the COOH terminus of the Cu-ATPase ATP7B in protein stability, trans-Golgi network retention, copper sensing, and retrograde trafficking. *Am J Physiol Gastrointest Liver Physiol*. 301:G69-81.

Braiterman, L.T., A. Gupta, R. Chaerkady, R.N. Cole, and A.L. Hubbard. 2015. Communication between the N and C Termini Is Required for Copper-stimulated Ser/Thr Phosphorylation of Cu(I)-ATPase (ATP7B). *The Journal of biological chemistry*. 290:8803-8819.

Braiterman, L.T., A. Murthy, S. Jayakanthan, L. Nyasae, E. Tzeng, G. Gromadzka, T.B. Woolf, S. Lutsenko, and A.L. Hubbard. 2014. Distinct phenotype of a Wilson disease mutation reveals a novel trafficking determinant in the copper transporter ATP7B. *Proc Natl Acad Sci U S A*. 111:E1364-1373.

Burd, C., and P.J. Cullen. 2014. Retromer: a master conductor of endosome sorting. *Cold Spring Harbor perspectives in biology*. 6.

Caca, K., P. Ferenci, H.J. Kuhn, C. Polli, H. Willgerodt, B. Kunath, W. Hermann, J. Mossner, and F. Berr. 2001. High prevalence of the H1069Q mutation in East German patients with Wilson disease: rapid detection of mutations by limited sequencing and phenotype-genotype analysis. *J Hepatol*. 35:575-581.

Canuel, L. S, Z. J, and M. CR. 2008. AP-1 and retromer play opposite roles in the trafficking of sortilin between the Golgi apparatus and the lysosomes. *Biochem Biophys Res Commun*. 366:724-730.

Chen, X., J. Kordich, E. Williams, N. Levine, A. Cole-Strauss, L. Marshall, V. Labrie, J. Ma, J. Lipton, and D. Moore. 2019. Parkinson's disease-linked D620N VPS35 knockin mice manifest tau neuropathology and dopaminergic neurodegeneration. *Proc Natl Acad Sci U S A.* .

Chen, Y., Y. Chang, M. Lan, P. Chen, and C. Lin. 2017. Identification of VPS35 p.D620N mutationrelated Parkinson's disease in a Taiwanese family with successful bilateral subthalamic nucleus deep brain stimulation: a case report and literature review. *BMC Neurol.* 17:191.

Cheng, X., Y. Xie, B. Zhou, N. Huang, T. Farfel-Becker, and Z. Sheng. 2018. Characterization of LAMP1-labeled nondegradative lysosomal and endocytic compartments in neurons.

. *J Cell Biol.* 217:3127-3139.

Cui, Y., J. Carosi, Z. Yang, N. Ariotti, M. Kerr, R. Parton, T. Sargeant, and R. Teasdale. 2019. Retromer has a selective function in cargo sorting via endosome transport carriers. *J Cell Biol.* 218:615-631.

Cullen, P.J., and H.C. Korswagen. 2012. Sorting nexins provide diversity for retromer-dependent trafficking events. *Nat Cell Biol*. 14:29-37.

Fahrni. 2013. Synthetic fluorescent probes for monovalent copper. *Curr Opin Chem Biol*. 17:656-662.

Feinstein, T., V. Wehbi, J. Ardura, D. Wheeler, S. Ferrandon, T. Gardella, and J. Vilardaga. 2011. Retromer terminates the generation of cAMP by internalized PTH receptors. *Nat Chem Biol.* . 7:278-284.

Follett, J., A. Bugarcic, Z. Yang, N. Ariotti, S. Norwood, B. Collins, R. Parton, and R. Teasdale. 2016. Parkinson's disease linked Vps35 R524W mutation impairs the endosomal association of retromer and induces α-synuclein aggregation. *J Biol Chem.* 291:18283-18298.

Francis, M., E. Jones, E. Levy, R. Martin, S. Ponnambalam, and A. Monaco. 1999. Identification of a di-leucine motif within the C terminus domain of the Menkes disease protein that mediates endocytosis from the plasma membrane. *J Cell Sci.* 112:1721-1732.

Fuse, A., N. Furuya, S. Kakuta, A. Inose, M. Sato, M. Koike, S. Saiki, and N. Hattori. 2015. VPS29–VPS35 intermediate of retromer is stable and may be involved in the retromer complex assembly process. *FEBS Lett.* . 589:1430-1436.

Gershlick, D.C., and M. Lucas. 2017. Endosomal Trafficking: Retromer and Retriever Are Relatives in Recycling. *Current biology : CB*. 27:R1233-R1236.

Gokool, S., D. Tattersall, J. Reddy, and M. Seaman. 2007. Identification of a conserved motif required for Vps35p/Vps26p interaction and assembly of the retromer complex. *Biochem. J*. 408:287-295.

Gupta, A., D. Aikath, R. Neogi, S. Datta, K. Basu, B. Maity, R. Trivedi, J. Ray, S.K. Das, P.K. Gangopadhyay, and K. Ray. 2005. Molecular pathogenesis of Wilson disease: haplotype analysis, detection of prevalent mutations and genotype-phenotype correlation in Indian patients. *Hum Genet*. 118:49-57.

Gupta, A., A. Bhattacharjee, O.Y. Dmitriev, S. Nokhrin, L. Braiterman, A.L. Hubbard, and S. Lutsenko. 2011. Cellular copper levels determine the phenotype of the Arg875 variant of ATP7B/Wilson disease protein. *Proceedings of the National Academy of Sciences of the United States of America*. 108:5390-5395.

Gupta, A., S. Das, and K. Ray. 2018. A glimpse into the regulation of the Wilson disease protein, ATP7B, sheds light on the complexity of mammalian apical trafficking pathways. *Metallomics*. 10:378-387.

Gupta, A., and S. Lutsenko. 2009. Human copper transporters: mechanism, role in human diseases and therapeutic potential. *Future Med Chem*. 1:1125-1142.

Gupta, A., M.J. Schell, A. Bhattacharjee, S. Lutsenko, and A.L. Hubbard. 2016. Myosin Vb mediates copper export in polarized hepatocytes. *J Cell Sci*.

Harada, M., S. Sakisaka, T. Kawaguchi, R. Kimura, E. Taniguchi, H. Koga, S. Hanada, S. Baba, K. Furuta, R. Kumashiro, T. Sugiyama, and M. Sata. 2000. Copper does not alter the intracellular distribution of ATP7B, a copper-transporting ATPase. *Biochem Biophys Res Commun*. 275:871-876.

Hierro, A., A. Rojas, R. Rojas, N. Murthy, G. Effantin, A. Kajava, A. Steven, J. Bonifacino, and J. Hurley. 2007. Functional architecture of the retromer cargo-recognition complex. *Nature*. 449:1063-1067.

665 Humphries, W.t., C. Szymanski, and C. Payne. 2011. Endo-Lysosomal Vesicles Positive for Rab7 and LAMP1 Are
666 Terminal Vesicles for the Transport of Dextran. *PlosOne*. 6.
667 Huster, D., and S. Lutsenko. 2007. Wilson disease: not just a copper disorder. Analysis of a Wilson disease model
668 demonstrates the link between copper and lipid metabolism. *Mol Biosyst*. 3:816-824.
669 Jain, S., G.G. Farias, and J.S. Bonifacino. 2014. Polarized Sorting of the Copper Transporter ATP7B in Neurons
670 Mediated by Recognition of a Dileucine Signal by AP-1. *Mol Biol Cell*.
671 Kambe. 2011. An overview of a wide range of functions of ZnT and Zip zinc transporters in the secretory pathway.
672 *Biosci Biotechnol Biochem*. 75:1036-1043.
673 Korolchuk, V.I., and D.C. Rubinsztein. 2011. Regulation of autophagy by lysosomal positioning. *Autophagy*. 7:927-
674 928.
675 Kurz, T., E. JW, and B. UT. 2011. The role of lysosomes in iron metabolism and recycling. *Int J Biochem Cell Biol.*
676 43(12):1686-1697.
677 LeShane, E.S., U. Shinde, J.M. Walker, A.N. Barry, N.J. Blackburn, M. Ralle, and S. Lutsenko. 2010. Interactions
678 between copper-binding sites determine the redox status and conformation of the regulatory N-terminal
679 domain of ATP7B. *The Journal of biological chemistry*. 285:6327-6336.
680 Lucas, M., D. Gershlick, A. Vidaurrazaga, A. Rojas, J. Bonifacino, and A. Hierro. 2016. Structural Mechanism for
681 Cargo Recognition by the Retromer Complex. *Cell* 167:1623-1635.
682 Lucas, M., and A. Hierro. 2017. Retromer. *Current biology : CB*. 27:R687-R689.
683 Lutsenko, S. 2016. Copper trafficking to the secretory pathway. *Metallomics*. 8:840-852.
684 Materia, S., M.A. Cater, L.W. Klomp, J.F. Mercer, and S. La Fontaine. 2012. Clusterin and COMMD1 independently
685 regulate degradation of the mammalian copper ATPases ATP7A and ATP7B. *The Journal of biological*
686 *chemistry*. 287:2485-2499.
687 McGough, I., F. Steinberg, M. Gallon, A. Yatsu, N. Ohbayashi, K. Heesom, M. Fukuda, and P. Cullen. 2014.
688 Identification of molecular heterogeneity in SNX27–retromer-mediated endosome-to-plasma-membrane
689 recycling. *J Cell Sci.* 127:4940-4953.
690 Mellado, M., Y. Cuartero, R. Brugada, and M. Verges. 2014. Subcellular localisation of retromer in post-endocytic
691 pathways of polarised Madin-Darby canine kidney cells. *Biol Cell.* 106:377-393.
692 Muchenditsi, A., H. Yang, J. Hamilton, L. Koganti, F. Housseau, L. Aronov, H. Fan, H. Pierson, A. Bhattacharjee, R.
693 Murphy, C. Sears, J. Potter, C. Wooton-Kee, and S. Lutsenko. 2017. Targeted inactivation of copper
694 transporter Atp7b in hepatocytes causes liver steatosis and obesity in mice. *Am J Physiol Gastrointest Liver*
695 *Physiol*. 313:G39-G49.
696 Otoikhian, A., A.N. Barry, M. Mayfield, M. Nilges, Y. Huang, S. Lutsenko, and N.J. Blackburn. 2012. Lumenal loop
697 M672-P707 of the Menkes protein (ATP7A) transfers copper to peptidylglycine monooxygenase. *Journal*
698 *of the American Chemical Society*. 134:10458-10468.
699 Petris, M.J., J. Camakaris, M. Greenough, S. LaFontaine, and J.F. Mercer. 1998. A C-terminal di-leucine is required
700 for localization of the Menkes protein in the trans-Golgi network. *Human molecular genetics*. 7:2063-
701 2071.
702 Polishchuk, E.V., M. Concilli, S. Iacobacci, G. Chesi, N. Pastore, P. Piccolo, S. Paladino, D. Baldantoni, I.S.C. van, J.
703 Chan, C.J. Chang, A. Amoresano, F. Pane, P. Pucci, A. Tarallo, G. Parenti, N. Brunetti-Pierri, C. Settembre,
704 A. Ballabio, and R.S. Polishchuk. 2014. Wilson disease protein ATP7B utilizes lysosomal exocytosis to
705 maintain copper homeostasis. *Dev Cell*. 29:686-700.
706 Priya, A., I. Kalaidzidis, Y. Kalaidzidis, D. Lambright, and S. Datta. 2015. Molecular insights into Rab7-mediated
707 endosomal recruitment of core retromer: deciphering the role of Vps26 and Vps35. *Traffic*. 16:68-84.
708 Rabanal-Ruiz, Y., and V.I. Korolchuk. 2018. mTORC1 and Nutrient Homeostasis: The Central Role of the Lysosome.
709 *International journal of molecular sciences*. 19.
710 Rahman, A., and B. Morrison. 2019. Contributions of VPS35 Mutations to Parkinson's Disease. *Neuroscience.*
711 401:1-10.
712 Reitz, C. 2018. Retromer Dysfunction and Neurodegenerative Disease. *Curr Genomics.* 19:279-288.

Rojas, R., T. van Vlijmen, G. Mardones, Y. Prabhu, A. Rojas, S. Mohammed, A. Heck, G. Raposo, P. van der Sluijs, and J. Bonifacino. 2008. Regulation of retromer recruitment to endosomes by sequential action of Rab5 and Rab7. *J Cell Biol.* 183:513-526.

Schneider, C., W. Rasband, and K. Eliceiri. 2012. NIH Image to ImageJ: 25 years of image analysis. . *Nat Methods*. volume9:671–675.

Seaman, M. 2007. Identification of a novel conserved sorting motif required for retromer-mediated endosome-to-TGN retrieval. *J Cell Sci*. 120:2378-2389.

Seaman, M.N.J. 2018. Retromer and Its Role in Regulating Signaling at Endosomes. *Progress in molecular and subcellular biology*. 57:137-149.

Shannon, B., A. Soto-Ortolaza, S. Rayaprolu, H. Cannon, C. Labbé, B. Benitez, J. Choi, T. Lynch, M. Boczarska-Jedynak, G. Opala, A. Krygowska-Wajs, M. Barcikowska, J. Van Gerpen, R. Uitti, W. Springer, C. Cruchaga, Z. Wszolek, and O. Ross. 2014. Genetic variation of the retromer subunits VPS26A/B-VPS29 in Parkinson's disease. *Neurobiol Aging.* . 35:1958.e1951-1952.

Small, S. 2008. Retromer Sorting: A Pathogenic Pathway in Late-Onset Alzheimer Diseas. *Arch Neurol.* 65:323-328.

Steinberg, F., M. Gallon, M. Winfield, E. Thomas, A. Bell, K. Heesom, J. Tavaré, and P. Cullen. 2013. A global analysis of SNX27–retromer assembly and cargo specificity reveals a function in glucose and metal ion transport. *Nat Cell Biol.* 15:461-471.

Suzuki, S., Y. Chuang, M. Li, M. Seaman, and S. Emr. 2019. A bipartite sorting signal ensures specificity of retromer complex in membrane protein recycling. *J Cell Biol.*

Suzuki, S., and S. Emr. 2018a. Membrane protein recycling from the vacuole/lysosome membrane. *J. Cell Biol*. 217:1623-1632.

Suzuki, S., and S. Emr. 2018b. Retrograde trafficking from the vacuole/lysosome membrane. *Autophagy*. 14:1654-1655.

Tabuchi, M., I. Yanatori, Y. Kawai, and F. Kishi. 2009. Retromer-mediated direct sorting is required for proper endosomal recycling of the mammalian iron transporter DMT1. *J Cell Sci.* 123:756-766.

Tammineni, P., Y.Y. Jeong, T. Feng, D. Aikal, and Q. Cai. 2017. Impaired axonal retrograde trafficking of the retromer complex augments lysosomal deficits in Alzheimer's disease neurons. *Human molecular genetics*. 26:4352-4366.

Team, R.D.C. 2015. R: A language and environment for statistical computing. .

Telianidis, J., Y.H. Hung, S. Materia, and S.L. Fontaine. 2013. Role of the P-Type ATPases, ATP7A and ATP7B in brain copper homeostasis. *Frontiers in Aging Neuroscience*. 5.

Uauy, R., M. Olivares, and M. Gonzalez. 1998. Essentiality of copper in humans. *Am J Clin Nutr*. 67:952S-959S.

Vardarajan, B., S. Bruesegem, M. Harbour, R. Inzelberg, R. Friedland, P. St George-Hyslop, M. Seaman, and L. Farrer. 2012. Identification of Alzheimer disease-associated variants in genes that regulate retromer function. *Neurobiol Aging.* 33:2231.e2215-2231.e2230.

Wen, L., F. Tang, Y. Hong, S. Luo, C. Wang, W. He, C. Shen, J. Jung, F. Xiong, D. Lee, Q. Zhang, D. Brann, T. Kim, R. Yan, L. Mei, and W. Xiong. 2011. VPS35 haploinsufficiency increases Alzheimer's disease neuropathology. *J Cell Biol.* . 195:765-779.

Wickham. 2009. Ggplot2 : elegant graphics for data analysis. *Springer*.

Zhang, J., C. Reiling, J. Reinecke, I. Prislan, L. Marky, P. Sorgen, N. Naslavsky, and S. Caplan. 2012. Rabankyrin-5 interacts with EHD1 and Vps26 to regulate endocytic trafficking and retromer function. *Traffic*. 13:745-757.

Zhao, X., S. Nothwehr, R. Lara-Lemus, B. Zhang, H. Peter, and P. Arvan. 2007 Dominant-negative behavior of mammalian Vps35 in yeast requires a conserved PRLYL motif involved in retromer assembly. *Traffic.* 8:1829-1840.

LEGENDS TO FIGURES

Fig1: **ATP7B recycles between TGN and vesicles in a copper dependent manner:** (A) Colocalization of ATP7B (green) with TGN marker, Golgin97 (red) in copper limiting, BCS (top panel) and 50µM copper (panel 2). Panel 3-5 shows subsequent return of vesicularized ATP7B upon BCS treatment for varying time length (10, 30 and 120mins). The overlap plots (right boxes) show the extent of overlap of green and red at lines drawn through the signals located on TGN (marked by arrow). Arrow and Arrowhead represents TGN localized and vesicularized ATP7B respectively. Scale bars represents 5µM. Blue signal represents DAPI staining for nucleus. (B) Pearson's correlation coefficient of colocalization between ATP7B and Golgin97 at different copper conditions demonstrated by a box plot with jitter points

Fig2: **ATP7B recycles from lysosome upon copper depletion:** (A) Colocalization of ATP7B (green) with lysosomal marker, lamp1 (red) in copper limiting, BCS (top panel) and 50µM copper (panel 2) and copper depletion post copper treatment (bottom panel). The overlap plots (right boxes) show the extent of overlap of green and red at lines drawn through the signals (marked by arrow or arrowhead). Arrowhead represents vesicularized ATP7B and arrow represents perinuclear positioned ATP7B. Scale bars represents 5µM. Blue signal represents DAPI staining for nucleus. (B) Pearson's correlation coefficient of colocalization between ATP7B and Lamp1 at different copper conditions demonstrated by a box plot with jitter points. (C) and (D) Comparative protein abundance of ATP7B (normalized against total membrane protein) determined by immunoblot at different copper and copper-depleted conditions (Cu: 50 µM and 250 µM and BCS: 50 µM).

Fig3: **ATP7B is preferentially located in Rab7-Lamp1 positive endosomes in high copper**: (A) Colocalization of ATP7B (cyan) with lysosomal marker, lamp1 (green) and late endosome marker, mCherry Rab7 (red) at 50µM copper. (B) 3D representation of Structured Illumination Microscopy (SIM) image of same with 100nm resolution. ATP7B is marked in magenta, Lamp1 in green and mCherry Rab7 in red. Arrow represents triple merging. Blue signal represents DAPI staining for nucleus.

Fig4: **ATP7B and VPS35 colocalizes at high copper:** (A) Immunoblot showing HepG2 expresses the retromer subunits VPS26 and VPS35 (B) Colocalization of ATP7B (green) with retromer subunit, VPS35 (red) in copper limiting, BCS (top panel) and 50µM copper (panel 2) and copper depletion post copper treatment (panels 3-4). The overlap plots (right boxes) show the extent of overlap of green and red at lines drawn through the signals (marked by arrow or arrowhead). Arrowhead represents vesicularized ATP7B and arrow represents perinuclear ATP7B. Scale bars represent 5µM. Blue signal represents DAPI staining for nucleus. (C) Pearson's correlation coefficient of colocalization between ATP7B and VPS35 at different copper conditions demonstrated by a box plot with jitter points

Fig5: **VPS35 regulates retrieval of ATP7B from lysosomes to TGN:** (A) siRNA mediated knockdown of Vps35 in HepG2 cells shows its downregulation. (*) denotes the VPS35 protein (B) Colocalization of ATP7B (green) with TGN marker, Golgin97 (red) in BCS (top panel) and 50µM copper (panel 2) and copper depletion post copper treatment (panels 3). Arrow denotes

TGN colocalization of ATP7B, Arrowhead denotes vesicularized ATP7B. Scale bars represent 5µM. (C) Pearson's correlation coefficient of colocalization between ATP7B and TGN at different copper conditions comparing VPS35 siRNA treated vs control demonstrated by a box plot. (D) Merged image showing colocalization of ATP7B (green) with Lamp1 (red) in high copper (top/bottom left) and copper depletion post copper treatment for 30 mins and 2h (top/bottom middle and right respectively). The top panel represents control cells transfected with scrambled siRNA and bottom panel represents cells with VPS35 siRNA. Arrows mark perinuclear ATP7B and arrowheads denote vesicular ATP7B (E) Localization of ATP7B (green) in VPS35 siRNA treated cells and subsequently transfected with mCherry-wtVPS35 (red). The left image represents cells that is not expressing mCherry-wtVPS35 (arrow represents vesicularized ATP7B) as compared to cells expressing the construct (arrowhead represents presence of tight perinuclear ATP7B). Cells belong to the same culture dish for both the images. Blue signal represents DAPI staining for nucleus.

Fig6: **Lysosomal luminal pH does not influence localization of ATP7B and recruitment of VPS35:** (A) Colocalization of ATP7B (green), Lamp1 (red) and VPS35 (cyan) in high copper for 2hrs in cells treated with Bafilomycin 1 (lower panel) or not (upper panel). (B) Colocalization of ATP7B (green), Lamp1 (red) and VPS35 (cyan) in cells treated with copper chelator for a brief period (20 mins) subsequent to high copper treatment to induce ATP7B vesicularization. Cells were treated with Bafilomycin 1 (lower panel) or not (upper panel).

Fig7: **ATP7B N-terminal ^{41}NVGY^{44} Δ mutant exhibits non-recycling phenotype:** Panel A: Colocalization of GFP-wtATP7B (green) with TGN marker, Golgin97 (red) shows ATP7B located on TGN in copper limiting, 50µM BCS (a), vesicularizes at 50µM copper (b) and subsequent return to TGN upon copper depletion post copper treatment (c). Panel B:The deletion mutant, ^{41}NVGY^{44} Δ GFP-ATP7B (green) shows localization with Golgin97 (red) in 50µM BCS (d), vesicularized at 50µM copper (e), primarily vesicularized ATP7B at Cu>BCS (f). Panel C: Colocalization of ^{41}NVGY^{44} Δ GFP-ATP7B (green), Lamp1 (red) and VPS35 (cyan). The construct remain perinuclear at 50µM BCS (g), colocalization of vesicularized ATP7B construct with Lamp1 and VPS35 at 50µM copper (h), remain vesicularized with similar colocalization of the ATP7B construct with Lamp1 and VPS35 as in 'h' (i). Blue signal represents DAPI staining for nucleus. Arrow denotes perinuclear ATP7B and arrowheads denote vesicularized ATP7B. Scale bars represent 5µM.

Fig8: **VPS35 interacts with ATP7B on lysosome in a micro-distant manner:** (A) High resolution deconvoluted confocal microscopy merged image showing colocalization of ATP7B (green) with Lamp1 (red) and VPS35 (blue) at 50µM copper. Grey represents nucleus. (B) Zoomed image of inset in A. The overlap plots (right box) show the extent of overlap of green, red and blue at lines drawn through the signals (marked by white line). (C) 3D representation of zoomed image in B, marked by dashed line. ATP7B is marked in green, Lamp1 in grey, VPS35 in magenta. Cyan represents nucleus. (D) 3D representation of Structured Illumination Microscopy (SIM) image of same with 100nm resolution. ATP7B is marked in green, Lamp1 in red and VPS35 in magenta. Arrowhead represents co-distribution of ATP7B and VPS35 in lysosomal compartment (Lamp1). (E) Stimulated emission depletion (STED) microscopy image

of ATP7B (green) and VPS35 (red). Top panel and bottom panel shows colocalization of ATP7B and VPS35 in high copper and copper depletion post copper treatment respectively. In both conditions ATP7B containing vesicles (marked by dotted circle) show juxta-positioning of VPS35 (red) and ATP7B (green). Arrowhead represents point of juxtaposition or merging. Scale bars represents 200nM.

Fig9: **Schematic representation of recycling of ATP7B between TGN and lysosomes.** Retromers are recruited on the lysosomal membrane that regulates retrograde transport of ATP7B upon copper removal.

Legends to supplementary figures

Fig S1: **Colocalization of ATP7B with late (Rab7) and mid (Rab11) endosomal markers at different copper levels:** (A) Colocalization of ATP7B (green) with late endosome marker, Rab7 (red) in copper limiting, BCS (top panel) and 50uM copper (panel 2) and copper depletion post copper treatment (bottom panel). Scale bars represents 5µM. Blue signal represents DAPI staining for nucleus. (B) Pearson's correlation coefficient of colocalization between ATP7B and Rab7 at different copper conditions demonstrated by a box plot. (C) Colocalization of ATP7B (green) with mid endosome marker, Rab11 (red) in copper limiting, BCS (top panel) and 50uM copper (panel 2) and copper depletion post copper treatment (bottom panel).

Fig S2 (A): **Immunoblot of VPS35 in different Copper conditions:** Upper panel shows abundance of VPS35 remain unchanged in all copper conditions. Lower panel shows the same for GAPDH, as a control for cytosolic proteins. (B) **Immunoblot of VPS26 in siVPS35 HepG2:** siRNA mediated knockdown of Vps35 in HepG2 cells shows downregulation of its core partner VPS26 as compared to its control. (*) denotes the VPS26 protein. (C) **VPS35 regulates retrieval of ATP7B from late endosome to TGN:** siVPS35 treated HepG2 cell shows colocalization of ATP7B (green) with Rab7 (red) in copper depletion post copper treatment for 30mins. Arrowhead shows ATP7B located in late endosomal vesicles and arrows shows non-returning vesicularized ATP7B. Scale bars represent 5µM. Blue signal represents DAPI staining for nucleus.

Fig S3: **Comparative dwell time analysis of ATP7B and wtVPS35 vs its mutant, VPS35 R107A**: Live-cell time-lapse high resolution deconvolution confocal microscopy shows dwell time of GFP-ATP7B with mCherry VPS35-WT to be ≈ 4 mins (A) and for mutant ≈ 3 seconds (B) in 50uM copper. Images were taken at every 1.93 s interval.

Fig S4: (A) **Alignment of the conserved putative sorting motifs at N-termini and C-termini (highlighted by red boxes) of ATP7B sequences amongst different organisms.** (B): *Table*; summarizing the results of trafficking studies of mutant ATP7B in different copper conditions.(c) **ATP7B sorting motif mutants shows mislocalized vesicular phenotype in every copper conditions:** Upper panel represents colocalization of C-terminal ^{1454}LLL^{1456}>AAA mutant (green) with TGN marker, Golgin97 (red) shows vesicularized fraction of ATP7B along with its TGN localization in copper limiting (BCS), high copper and copper depletion post copper treatment . Middle panel represents C-terminal (1373-1384) three tandem YXXΦ Δ (green)

shows leaky vesicularized phenotype with a commendable portion to be retained on endoplasmic reticulum. Lower panel represents N-terminal N41S mutant shows vesicularized pattern in all three copper conditions. Blue signal represents DAPI staining for nucleus. Arrowhead denotes vesicularized ATP7B.

Fig S5: (A) **Co-purification assay to determine the interaction between domains of ATP7B and retromer components** (i) Empty pGEX and pGEX-N-term ATP7B were expressed in BL21 and lysates were incubated with GSH beads. Coomassie stained gels showing the proteins in lysates and flow through as indicated. (ii) Empty BL21 and transformed BL21 containing pET28aSUMO with C-term ATP7B lysates were incubated with Ni-sepharose beads. Coomassie stained gels showing the proteins in lysates and flow through as indicated. (iii) and (iv) HepG2 whole cell lysates were incubated with the C-term ATP7B bound Ni-sepharose beads. Eluted products were analysed by immunoblotting as indicated. (v) and (vi) HepG2 whole cell lysates were incubated with the N-term ATP7B bound GSH beads. Eluted products were analysed by immunoblotting as indicated. (B) **Co-immunoprecipitation assay to determine the interaction between full length ATP7B and VPS35:** Cell was transfected with GFP-ATP7B and treated with different copper conditions as mentioned. Lysates were incubated with GFP-trap beads. Untransfected cells were used as negative control. vii) Immunoblot showing the presence of GFP-ATP7B in whole cell lysates and GFP-trap beads after elution. viii) GFP-trap immune-co-precipitated products were subjected to immunoblot as indicated. Abbreviations: *FT: Flow through; WCL: Whole cell lysate, E: Eluate.*

904 Figures Fig1

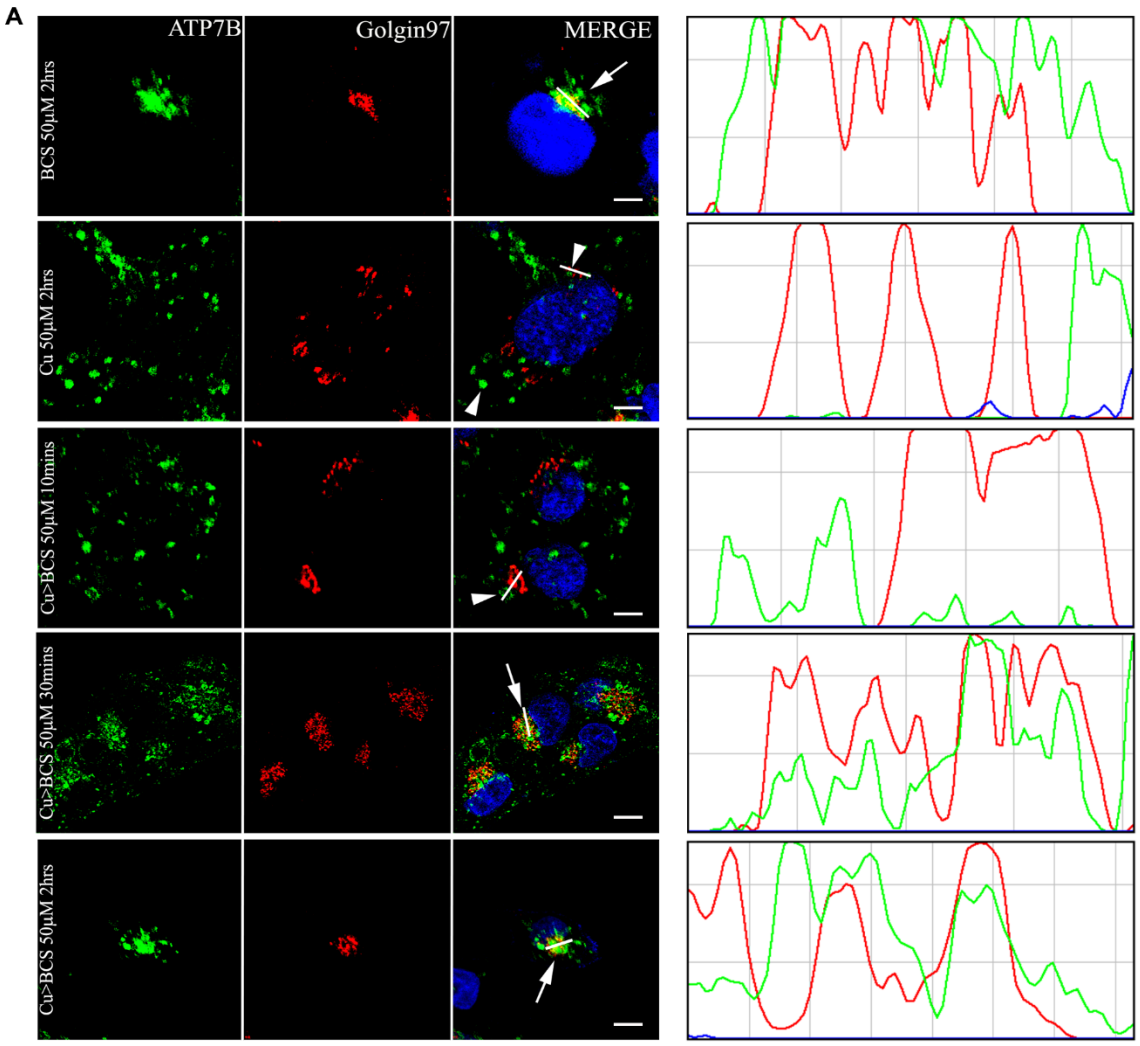

905

906 Fig. 2

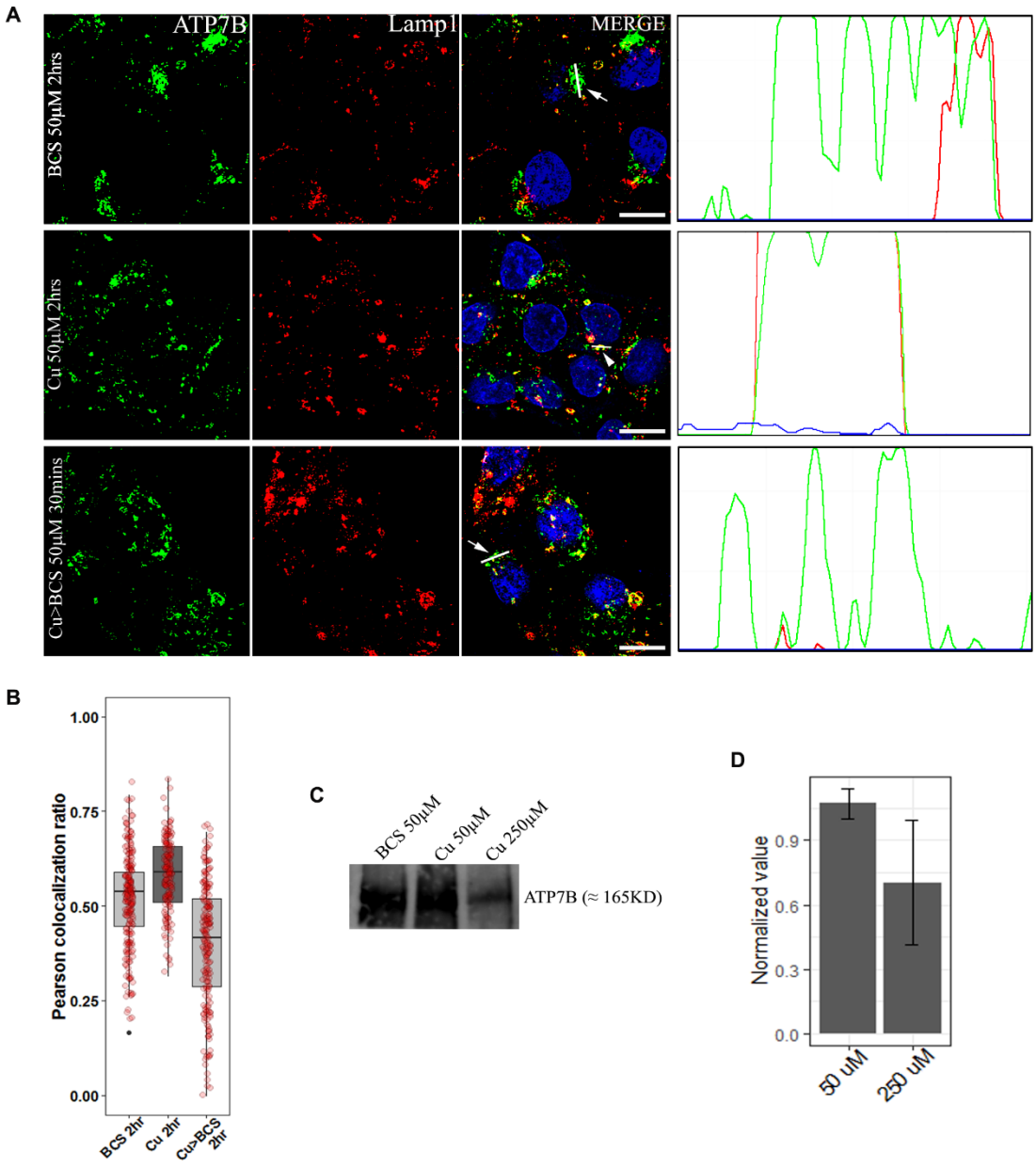

907

908

909 Fig. 3

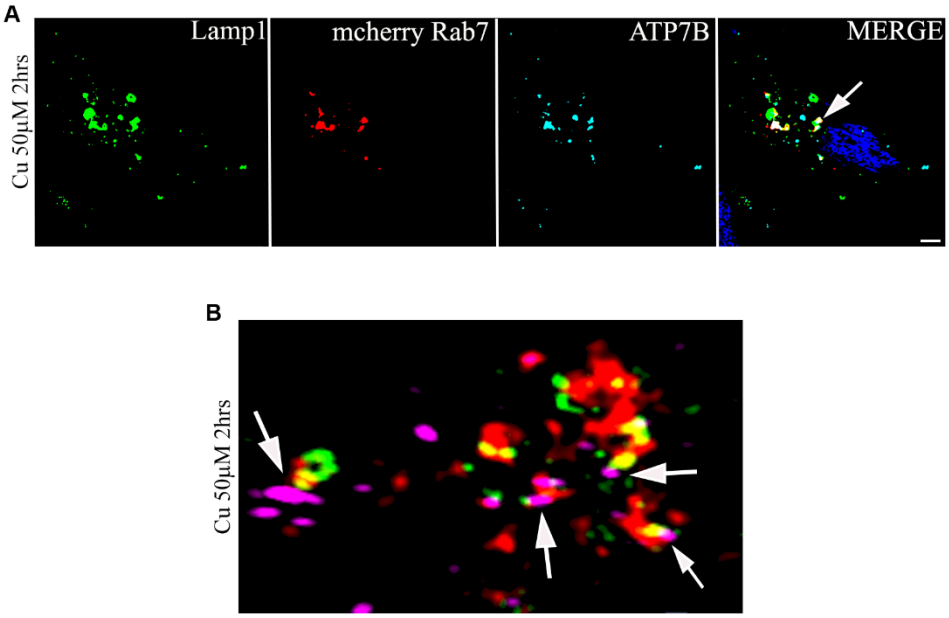

910

911

912 Fig. 4

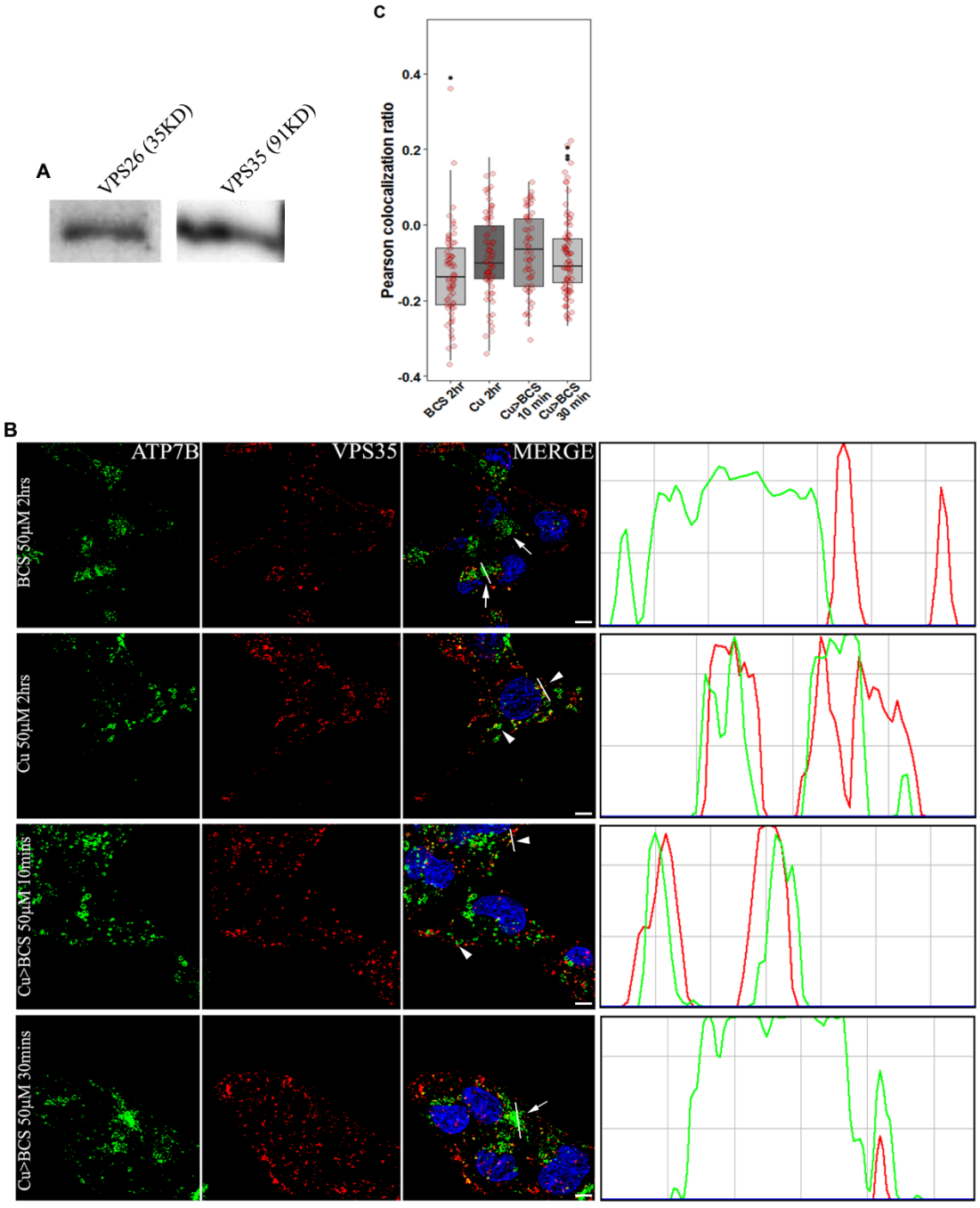

913

914

Fig. 5

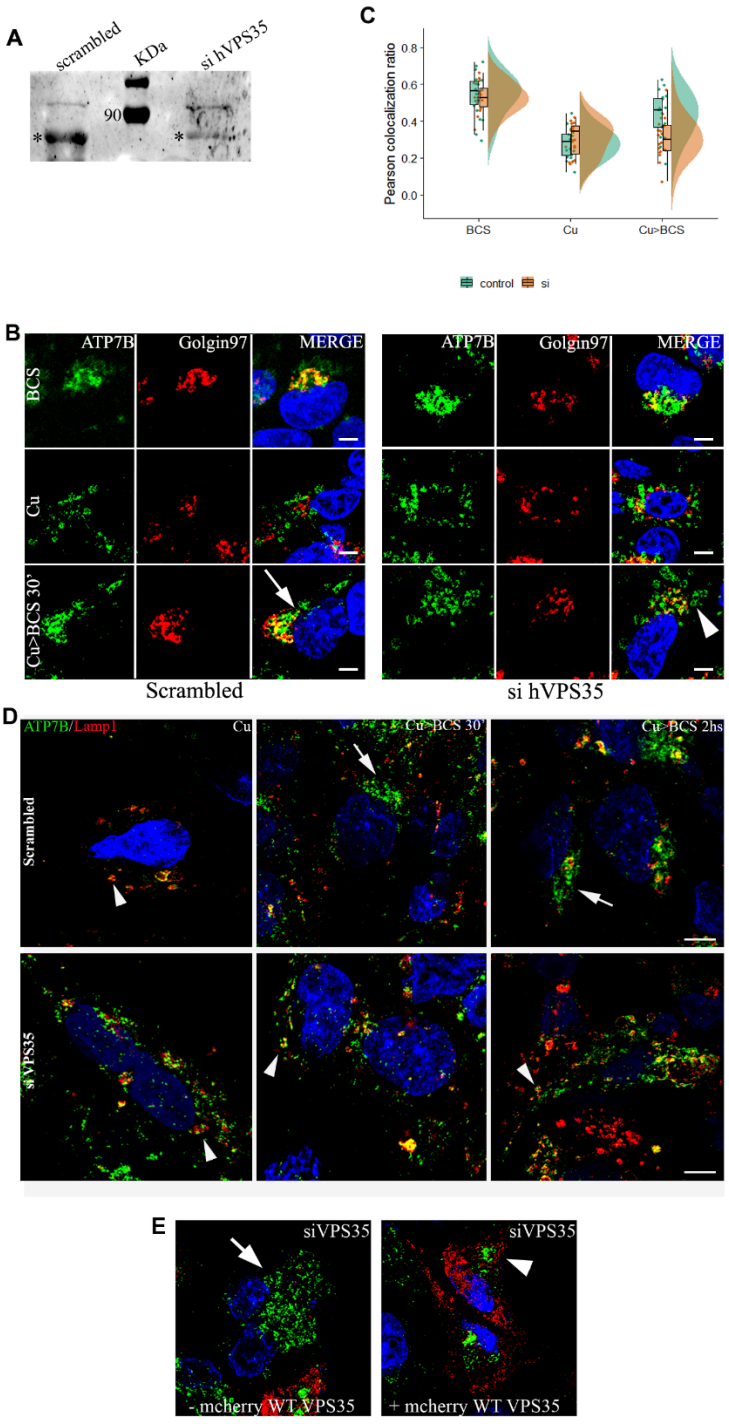

Fig. 6

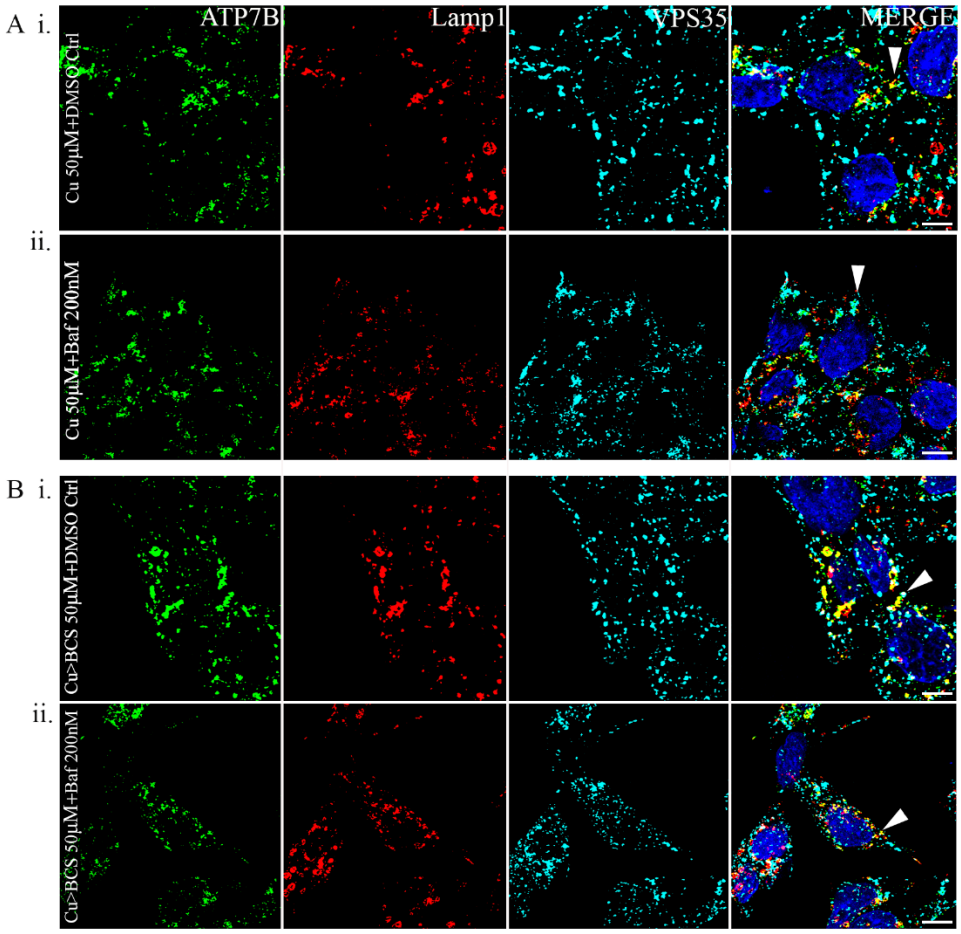

921 Fig. 7

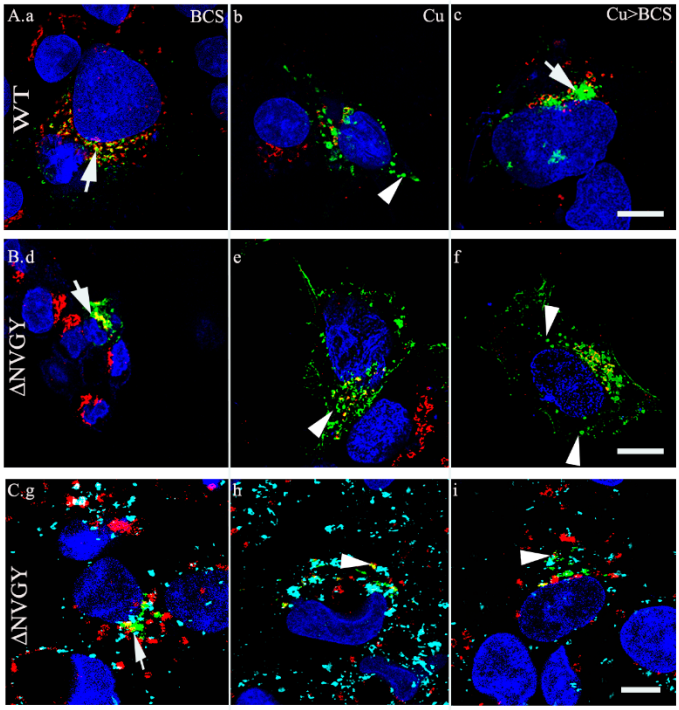

922

923

924 Fig. 8

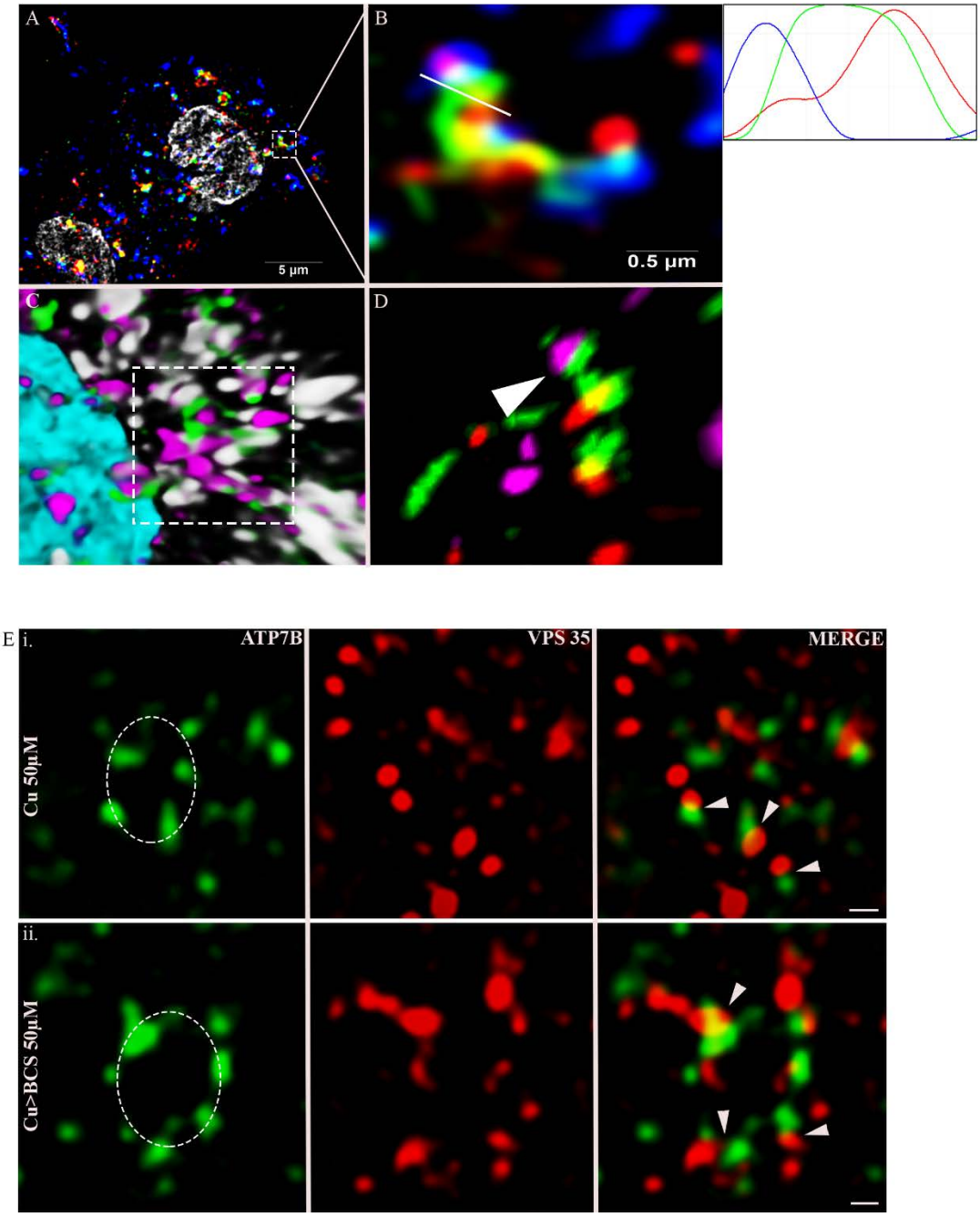

925

926

927 Fig. 9

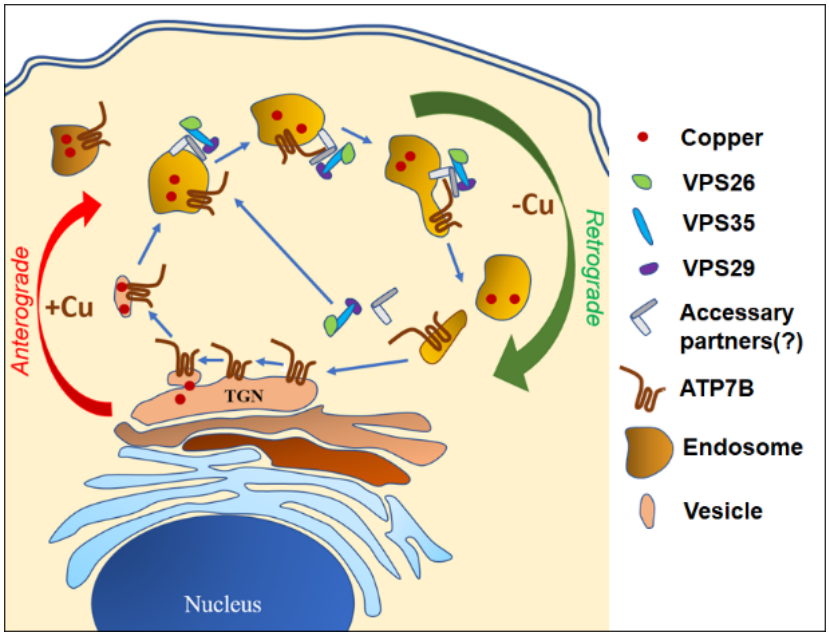

928

929

930

Supplementary Figs

Fig. S1

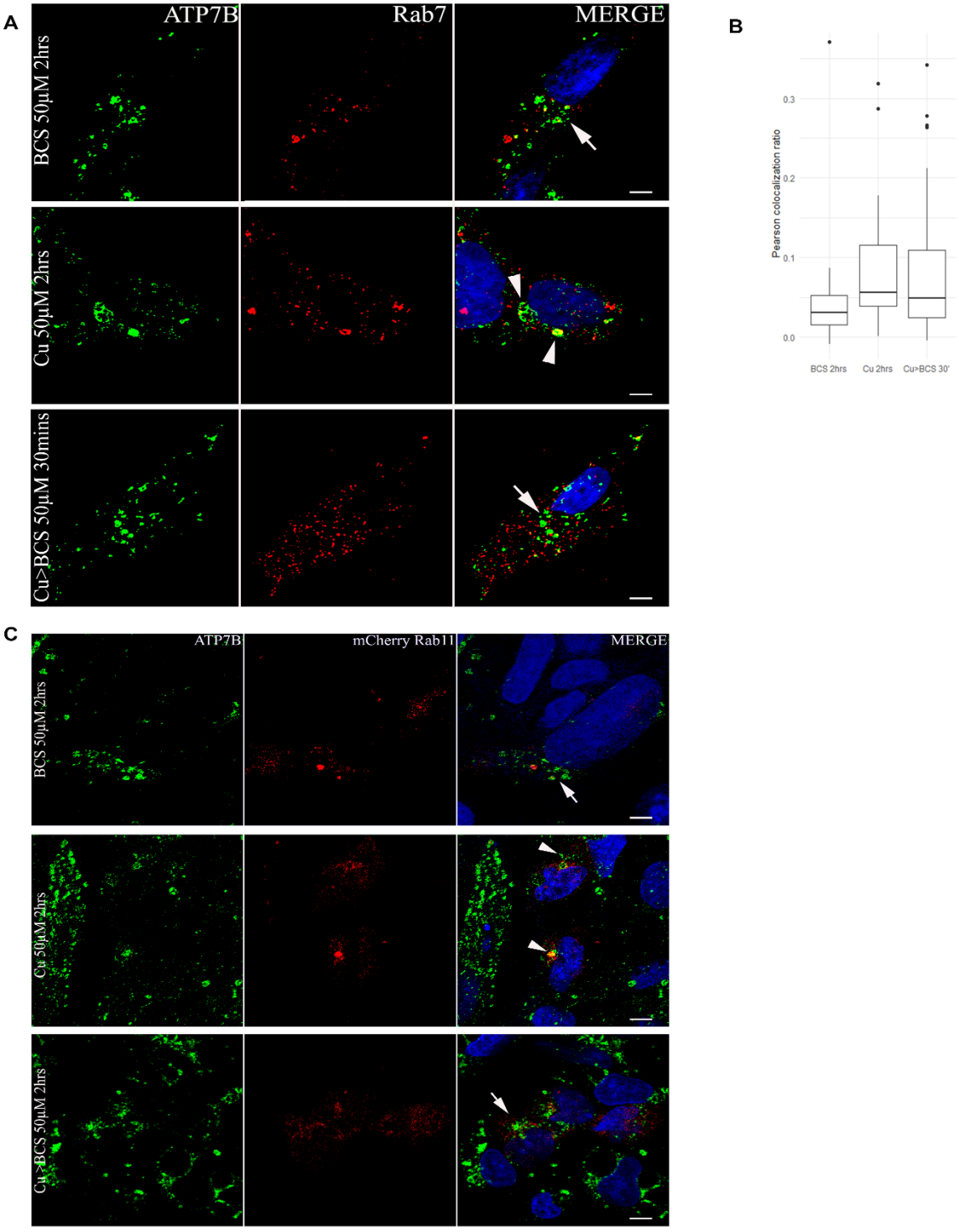

935 Fig. S2

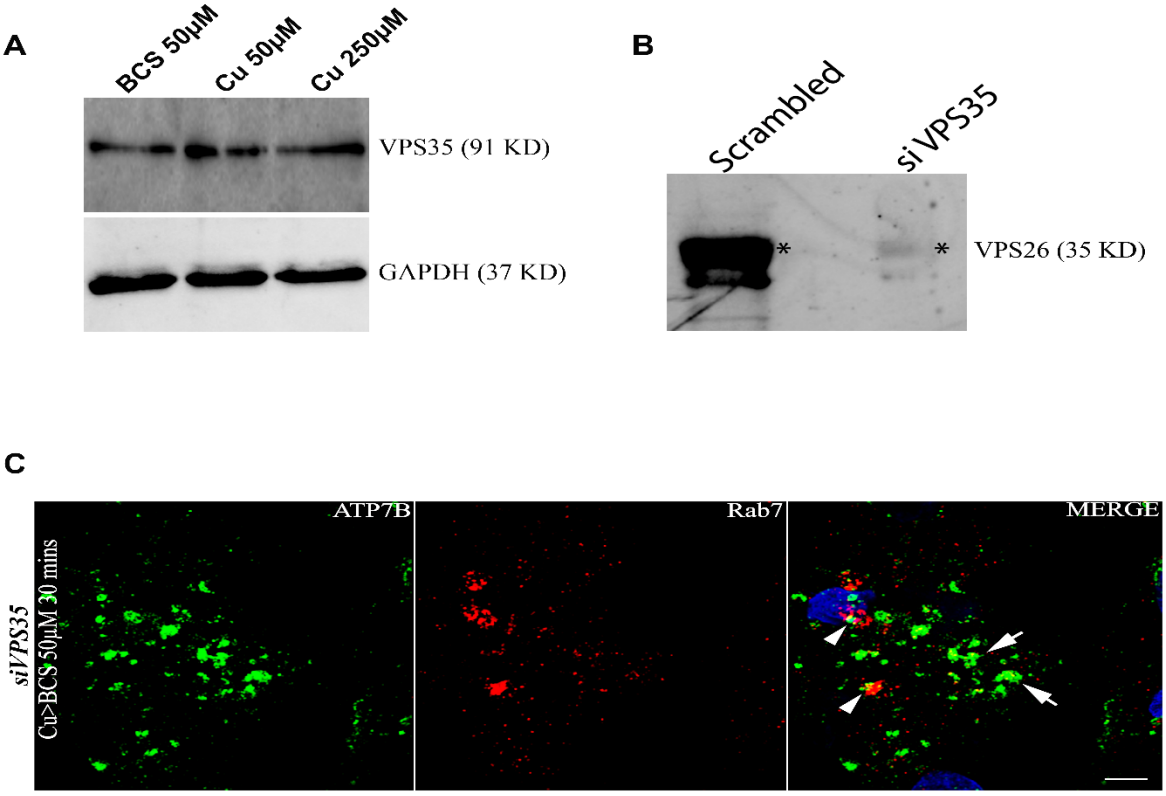

936

937

938 Fig. S3

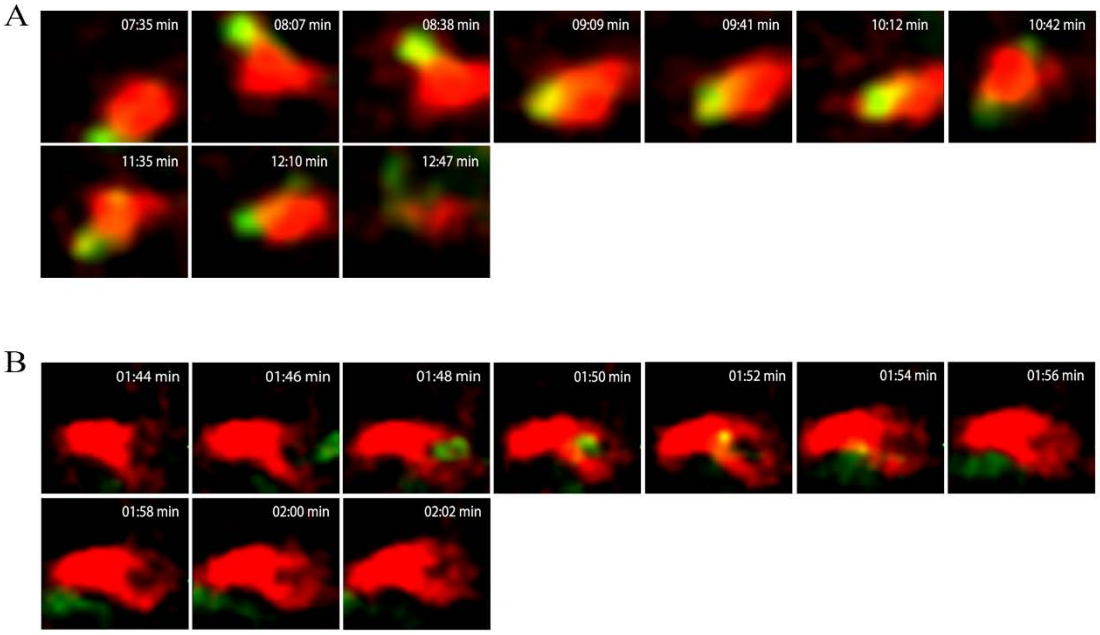

939

940

941 Fig. S4

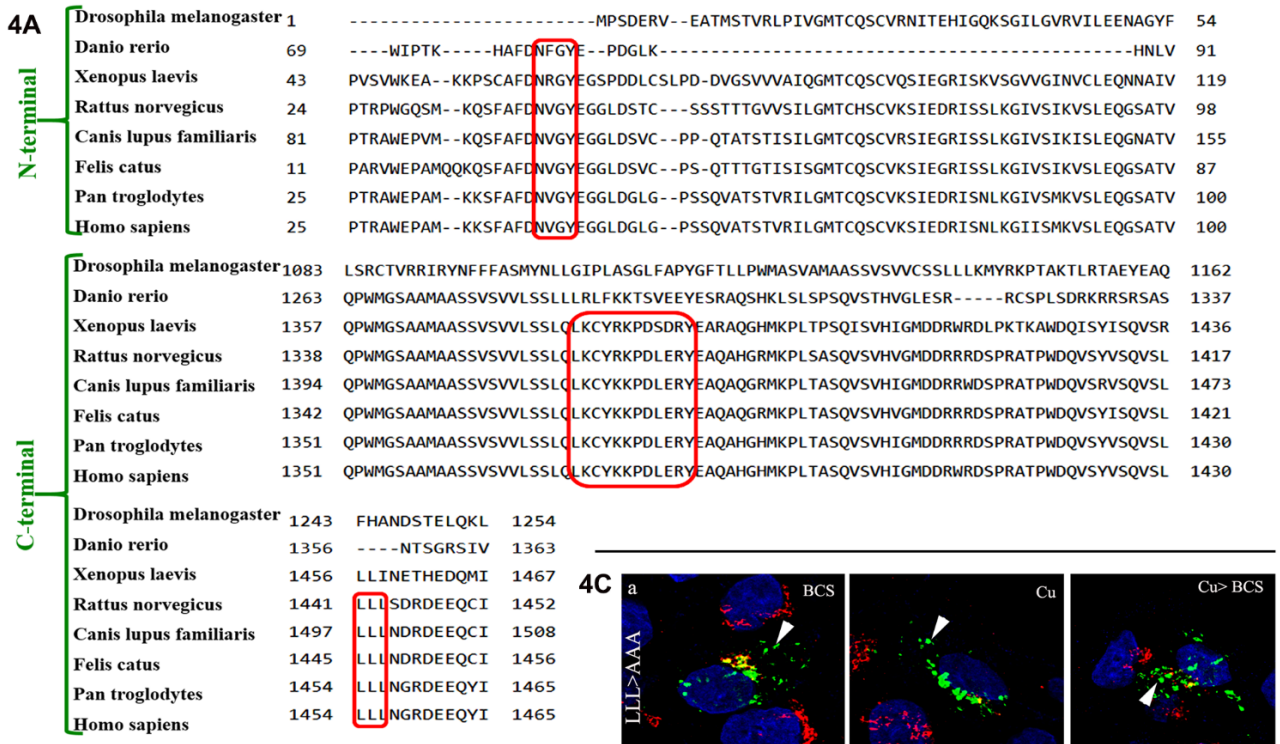

4B

Domains	Sorting Motifs	Mutants	BCS 50μM	Cu 50μM	Cu > BCS (50μM)
N-terminal	^{41}NVGY^{44}	Δ	TGN	Vesicularised	Vesicularised
		N41S	TGN+Vesicularised	Vesicularised	Vesicularised
		Y44V	ER Retention	ER Retention	ER Retention
		Y44D	ER Retention	ER Retention	ER Retention
C-terminal	^{1373}LKCYKKPDLERY^{1384}	Δ	ER Retention	ER Retention	ER Retention
		Y1376V	Vesicularised	Vesicularised	Vesicularised
		Y1376D	Vesicularised	Vesicularised	Vesicularised
	^{1454}LLL^{1456}	LLL>AAA	Vesicularised	Vesicularised	Vesicularised

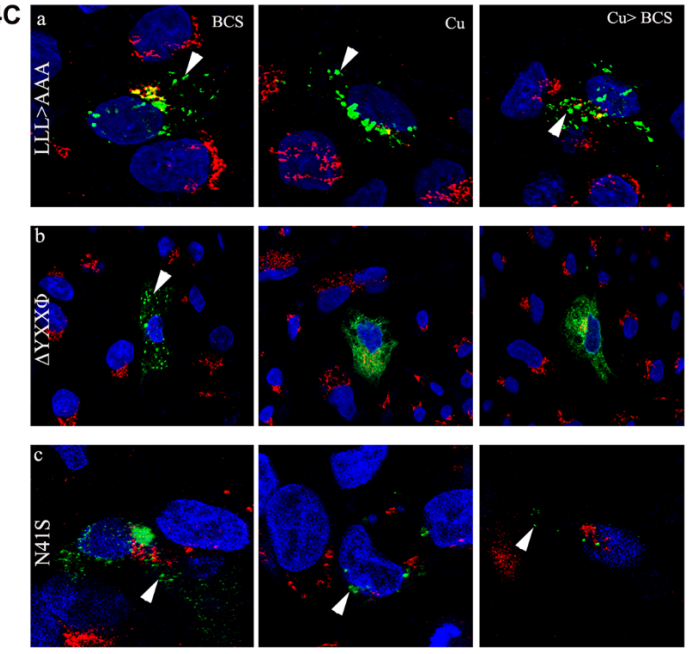

942

943

944 Fig. S5

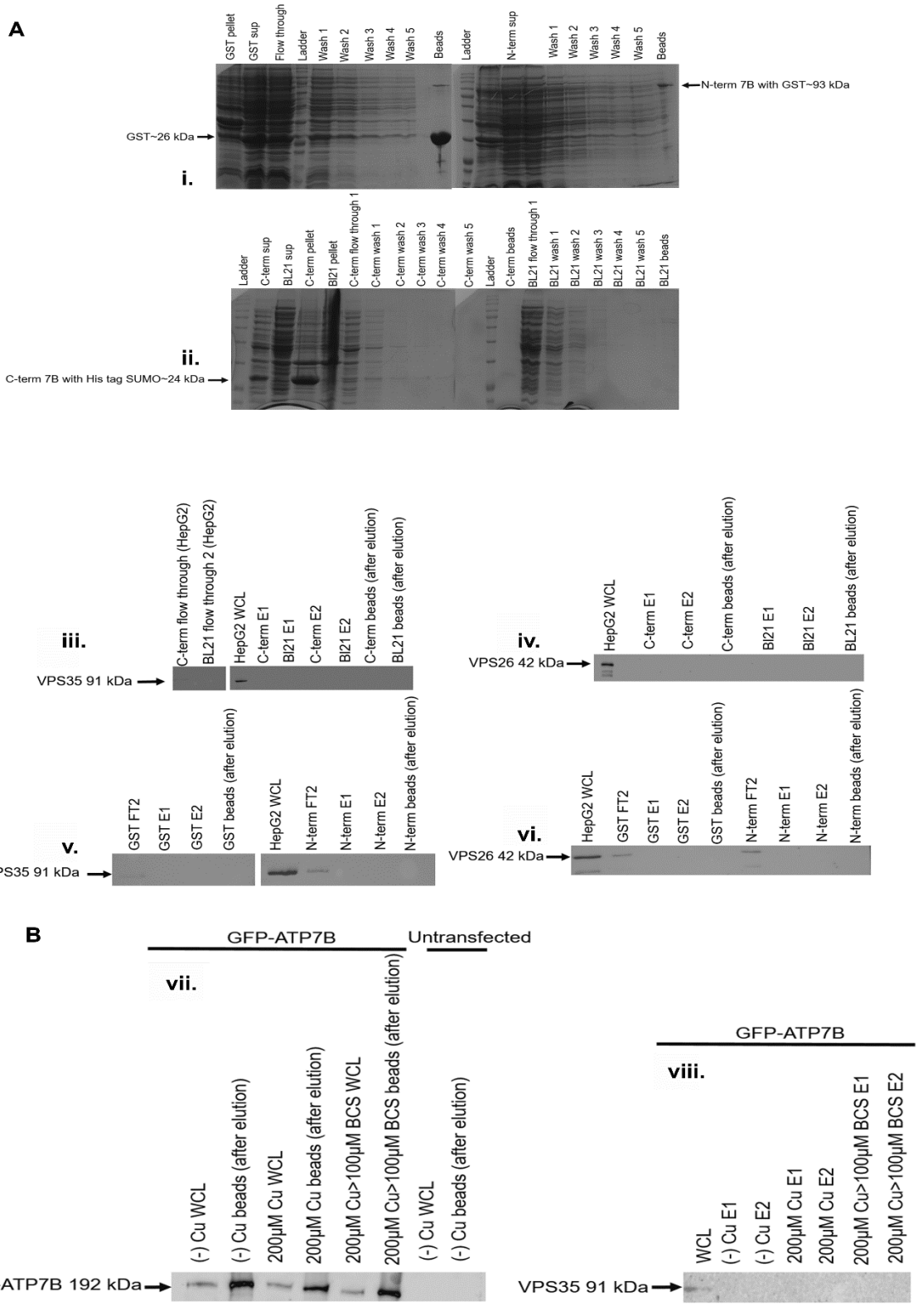

945

946

947